

1-1-2004

Modeling of inclusion removal in a tundish by gas bubbling

John Patrick Rogler
Ryerson University

Follow this and additional works at: <http://digitalcommons.ryerson.ca/dissertations>

 Part of the [Chemical Engineering Commons](#)

Recommended Citation

Rogler, John Patrick, "Modeling of inclusion removal in a tundish by gas bubbling" (2004). *Theses and dissertations*. Paper 54.

This Thesis is brought to you for free and open access by Digital Commons @ Ryerson. It has been accepted for inclusion in Theses and dissertations by an authorized administrator of Digital Commons @ Ryerson. For more information, please contact bcameron@ryerson.ca.

MODELING OF INCLUSION REMOVAL IN A TUNDISH BY GAS BUBBLING

by

John Patrick Rogler, B. Eng. Ryerson University, 2001

A thesis

presented to Ryerson University

in partial fulfillment of the

requirements for the degree of

Master of Applied Science

in the Program of

Chemical Engineering

Toronto, Ontario, Canada, 2004

©John Patrick Rogler 2004



Library and
Archives Canada

Bibliothèque et
Archives Canada

Published Heritage
Branch

Direction du
Patrimoine de l'édition

395 Wellington Street
Ottawa ON K1A 0N4
Canada

395, rue Wellington
Ottawa ON K1A 0N4
Canada

Your file *Votre référence*

ISBN: 0-494-08196-1

Our file *Notre référence*

ISBN: 0-494-08196-1

NOTICE:

The author has granted a non-exclusive license allowing Library and Archives Canada to reproduce, publish, archive, preserve, conserve, communicate to the public by telecommunication or on the Internet, loan, distribute and sell theses worldwide, for commercial or non-commercial purposes, in microform, paper, electronic and/or any other formats.

The author retains copyright ownership and moral rights in this thesis. Neither the thesis nor substantial extracts from it may be printed or otherwise reproduced without the author's permission.

AVIS:

L'auteur a accordé une licence non exclusive permettant à la Bibliothèque et Archives Canada de reproduire, publier, archiver, sauvegarder, conserver, transmettre au public par télécommunication ou par l'Internet, prêter, distribuer et vendre des thèses partout dans le monde, à des fins commerciales ou autres, sur support microforme, papier, électronique et/ou autres formats.

L'auteur conserve la propriété du droit d'auteur et des droits moraux qui protègent cette thèse. Ni la thèse ni des extraits substantiels de celle-ci ne doivent être imprimés ou autrement reproduits sans son autorisation.

In compliance with the Canadian Privacy Act some supporting forms may have been removed from this thesis.

Conformément à la loi canadienne sur la protection de la vie privée, quelques formulaires secondaires ont été enlevés de cette thèse.

While these forms may be included in the document page count, their removal does not represent any loss of content from the thesis.

Bien que ces formulaires aient inclus dans la pagination, il n'y aura aucun contenu manquant.


Canada

I hereby declare that I am the sole author of this thesis.

I authorize Ryerson University to lend this thesis to other institutions or individuals for the purpose of scholarly research.

John Patrick Rogler

I further authorize Ryerson University to reproduce this thesis by photocopying or by other means, in total or parts, at the request of other institutions or individuals for the purpose of scholarly research.

John Patrick Rogler

Borrower's Page

Ryerson University requires the signatures of all persons using or photocopying this thesis. Please sign below, and give address and date.

Abstract

MODELING OF INCLUSION REMOVAL IN A TUNDISH BY GAS BUBBLING

Master of Applied Science, 2004

John Patrick Rogler, Department of Chemical Engineering, Ryerson University

Inclusion removal from liquid steel by attachment to rising gas bubbles has been reviewed. A mathematical model of inclusion removal by gas bubbling in a tundish has been developed and it is found that minimization of bubble size is critical to enhance removal. However, small bubble formation in a tundish may be problematic as bubble size is controlled by high contact angles between liquid metal and bubble orifice materials. A physical modeling technique has been developed to simulate inclusion removal by tundish bubbling. The influence of a floating particle sink, a flow pattern modifying impact pad, and a bubbler, on particle separation was examined. The influence of gas flow rate, tundish residence time, particle size and bubble size was also examined. Physical modeling confirms that particle separation by gas bubbling in a tundish can be efficient at enhancing inclusion removal. It was also confirmed that relatively small bubbles (<1mm in diameter) are required for maximum separation efficiency.

Acknowledgments

I would like to thank my supervisors, Dr. Larry Heaslip and Dr. Mehrab Mehrvar for their support in this project. I would also like to thank everyone at Advent Process Engineering Inc., for their constant supply of help and knowledge, especially Dr. Larry Heaslip without whom this paper would not have been possible. I extend special thanks to Professor Alexander Penlidis of the Department of Chemical Engineering of the University of Waterloo for the analysis of the Polyethylene sample. Thanks to my parents for their love and support.

Table of Contents

	Page
Author's Declaration	ii
Borrowers Page	iii
Abstract	iv
Acknowledgements	v
Table of Contents	vi
List of Tables	viii
List of Figures	viii
Nomenclature	ix
1.0 INTRODUCTION	1
2.0 LITERATURE REVIEW	4
2.1 Particle/Bubble Collision and Attachment	5
2.2 Bubble Rise Velocity	9
2.3 Capillary Effects On Inclusion Flotation	10
3.0 MATHEMATICAL MODEL OF TUNDISH BUBBLING	12
3.1 Development of Mathematical Model	12
3.2 Interpretation of Mathematical Model Results	16
3.2.1 Minimum Bubble Size	16
3.2.2 Control of Bubble Size	17
3.2.3 Novel Designs For Non-Wetted Slot	20
3.3 Discussion of Mathematical Model Results	21
4.0 EXPERIMENTAL METHOD - PHYSICAL MODELING	23
4.1 Physical Model Apparatus	23
4.2 Experimental Approach	24
5.0 TUNDISH RTD MEASUREMENTS	29
6.0 PARTICLE SEPARATION RESULTS	31
6.1 Initial Physical Modeling	31
6.2 Primary Matrix of Physical Modeling Experiments	32
6.2.1 Baseline	33
6.2.2 Impact Pad	34
6.2.3 Tundish Bubbling	35
6.2.4 Impact Pad and Tundish Bubbling	38
6.3 Comparison of Physical and Mathematical Modeling	39
6.3.1 Influence of Gas Flow Rate	39
6.3.2 Influence of Particle Size	41

6.3.3	Influence of Tundish Residence Time	42
6.3.4	Influence of Gas Bubble Size	43
7.0	CONCLUSION AND RECOMMENDATIONS	45
8.0	REFERENCES	47
9.0	APPENDICES	49
9.1	Froude Number Similitude	49
9.2	Simulation of Particle Rise Velocity Based on Stoke's Law	51
9.3	Simulation of Oxide Inclusion Concentration in Liquid Steel	52
9.4	Dimensionless Parameters	53
9.5	Analysis of Polyethylene Particles	54

List of Tables

Table	Description	Page
1	Primary Experimental Matrix	32
A1	Average molecular weights of LLDPE sample	54

List of Figures

Figure	Description	Page
A1	Comparison of GPC Results	56
A2	CRYSTAF Results	56
1	Schematic of Tundish Equipped with Bubbling Block for Enhanced Inclusion Removal	57
2	Schematic of Critical Angles	57
3	Influence of Bubble Size on Collision Probability	58
4	Influence of Bubble Size on Particle Collection Probability	58
5	Schematic of Tundish Bubbling Model	59
6	Influence of Bubble Size, Bubbly Volume Fraction and Particle Size on Inclusion Removal Efficiency	59
7	Influence of Bubble Size, Bubbly Volume Fraction and Tundish Residence Time on Inclusion Removal Efficiency	60
8	Schematic of Bubble Formation on Wetted and Non-wetted Nozzles	60
9	Internal Dimensions of Single Strand Tundish Model	61
10	Schematic of Apparatus	61
11	Dimensions of Bubbling Block	62
12	Comparison of RTD in Tundish with No Furniture to Tundish with Impact Pad and Conventional Dam	62
13	Comparison of RTD in Tundish with No Furniture to Tundish with Tundish Bubbler	63
14	Comparison of RTD in Tundish with No Furniture to Tundish with Impact Pad and Tundish Bubbler	63
15	Results of Primary Experimental Matrix	64
16	Comparison of Bubbles Before and During Interaction with Particles	64
17	Schematic Illustrating Large Scale Eddy Formed by Bubbling in the tundish	65
18	Influence of Gas Injection Rate on Particle Separation Efficiency	65
19	Influence of Particle Size on Particle Separation Efficiency	66
20	Influence of Tundish Throughput on Particle Separation Efficiency	66
21	Influence of Bubble Size and Gas Injection Rate on Particle Separation Efficiency	67

Nomenclature

- A Dimensionless Parameter in equation 4 (also see Appendix 9.4)
- A_{BS} Area of Bubble Source (m^2)
- A_S Area of Shroud (m^2)
- B Dimensionless Parameter in equation 4 (also see Appendix 9.4)
- C Dimensionless Parameter in equations 1 and 10 (also see Appendix 9.4)
- D Dimensionless Parameter in equations 3 and 10 (also see Appendix 9.4)
- d_B Diameter of Bubble (m)
- d_o Orifice Diameter (m)
- $d_{n,o}$ Outer Diameter of Orifice Block (m)
- d_p Particle (Inclusion) Diameter (m)
- g Acceleration due to Gravity ($9.81 m/s^2$)
- H Height of liquid metal in the vessel = 1m in the present study
- h_{Cr} Critical Film Thickness (m)
- k Constant in equation 7 (1/s)
- K Rate constant
- L Length of the tundish (m)
- L_c Characteristic Length (m)
- L_B Length of Bubbly Region in the tundish (m)
- $L_{,min}$ Minimum distance between bubble source block and the tundish outlet (m)
- M Dimensionless Parameter used to calculate A (also see Appendix 9.4)
- N Dimensionless Parameter used to calculate B (also see Appendix 9.4)

n Number of particles per unit volume at time (t), (m^{-3})
 n_o Initial number of particles per unit volume at time (t=0), (m^{-3})
 N_B Number of bubbles supplied to liquid steel bath per unit time and volume ($\text{m}^{-3}\text{s}^{-1}$)
 N_{CC} Number of collecting collisions
 $N_{Re,o}$ Orifice Reynolds Number
 N_T Total Number of collecting collisions
 P Particle collection probability ($P = P_{at} \cdot P_c$)
 P_{at} Bubble-particle attachment probability
 P_f Film thinning probability
 P_C Collision probability
 P_{det} Detachment probability
 Q Gas flow rate (m^3/s)
 Q_L Liquid flow rate (m^3/s)
 q_G Gas flow rate per unit area of bubble source ($\text{m}^3/\text{s} \cdot \text{m}^2$)
 Re_b Reynolds Number for Bubbles ($d_{BUB}\rho_L/\mu$)
 t time (s)
 t_C Collision time (s)
 t_{FC} Film drainage and rupture time during sliding (s)
 t_i Induction time (s)
 t_s Sliding time (s)
 T_F Temperature of steel (K)
 T_o Temperature of gas at the flow meter (K)
 u_B Bubble rise velocity (m/s)

- $u_{B,min}$ Minimum bubble rise velocity (m/s)
- u_L Liquid velocity in the tundish (m/s)
- u_P Particle (Inclusion) rise velocity (m/s)
- V Volume of liquid steel = 1 m³ in the present study
- V_B Volume of bubble (m³)
- V_{BC} Volume of bubble column (m³)
- X Dimensionless Parameter in equations 1 and 10 (also see Appendix 9.4)
- Y Dimensionless Parameter in equations 1 and 10 (also see Appendix 9.4)

Greek Symbols

- α Central angle for the contact of inclusion and bubble
- ε Inclusion Removal Efficiency
- η Inclusion Removal Efficiency
- μ Viscosity of the Liquid (Ns/m²)
- ρ_G Density of the Gas (kg/m³)
- ρ_L Density of the Liquid (kg/m³)
- ρ_s Density of the solid (inclusion) (kg/m³)
- θ_A Maximum adhesion angle, beyond which no adhesion happens
- θ_C Maximum collision angle, beyond which no collision happens
- θ_m Angle at which the inclusion stop to slide on the bubble surface
- θ_O Angle at which the inclusion starts to slide on the bubble surface
- σ Surface Tension (N/m)
- τ Residence time of the liquid in the bubbly region (s)
- τ_T Residence time of the liquid in the tundish (s)

1.0 INTRODUCTION

The removal of suspended or entrained particles from a liquid by attachment to rising gas bubbles is a separation process implemented in various industries to separate a particulate phase from a liquid bulk. In particular, the removal of buoyant non-metallic inclusions from liquid steel baths is an important practice in primary steel production. Non-metallic inclusions, such as sulphide, silicate and aluminate particles, are formed in the steelmaking process. These inclusions, if they are large enough and entrapped within the steel matrix, may lead to undesirable defects in steel products. For steel to be termed 'clean', it must have a low level of residual inclusion particles. The consumers of high quality steels often set stringent tolerances on the cleanliness of the steel they purchase and thus the production of clean steels is a often goal of critical primary steel producers.

Argon gas injection into a ladle of liquid steel to induce thermal homogeneity of the metal bath by stirring and to improve the separation efficiency of non-metallic particles is a common practice used during steelmaking [1,2]. However after ladle treatment, liquid steel is generally poured from the ladle into the tundish as part of the continuous casting process and during this pouring, inclusions may be re-introduced into the molten metal. The tundish provides another location for inclusion separation and it would be beneficial to enhance particle separation in the tundish. To accomplish this, inert gas could be introduced from a porous plug located between the inlet and outlet of the tundish as seen in Fig. 1. This process could be as follows: (1) liquid steel flows into the tundish, (2) the combination of inclusions carried over from the ladle and inclusions formed by reaction

with air or slag during steel pouring determines the concentration and size distribution of inclusions in the inlet region of the tundish, (3) the steel flow passes through the bubbly region of the tundish, (4) liquid steel passage through the bubbly region accelerates the separation of particles from the liquid metal into the floating slag layer, and (5) the metal flow exiting the tundish has an inclusion population of reduced size and number as compared to the inlet region of the tundish. Accelerated particle separation by gas bubbling may be the result of; (a) particle/bubble collisions leading to particle/bubble attachment and rapid transport of the attached particles to the slag layer by the rising bubbles, (b) rising bubbles carrying the liquid metal and entrained buoyant particles upward toward the slag layer where the particles can separate by buoyancy, and (c) an enhanced rate of particle/particle collisions as induced by the turbulence in the bubble plume, generated by the rising bubbles leading to larger, and thus more buoyant, particle agglomerations.

The probabilities of inclusion removal from liquid steel by collision and attachment to rising gas bubbles have been analyzed and reviewed. This analysis is presented in the Literature Review (Section 2 of this thesis). A simple mathematical model of inclusion removal by gas bubbling in a tundish has been developed and is presented in Section 3. It is found that bubble size in the range of 0.5 to 3 mm should provide a useful level of inclusion removal efficiency while allowing complete bubble separation from the liquid metal in the tundish (i.e. without bubble carryover in the tundish exit flow). Increasing the bubbly volume fraction in the tundish and the tundish residence time can be used to improve the inclusion removal efficiency by gas bubbling. However, the formation of

the small bubbles (0.5 to 3mm diameter) necessary to accelerate inclusion removal in a tundish may be problematic as bubble size is affected by the high wetting angles typical of liquid metal contact with porous refractories.

A physical modeling apparatus and technique have been developed to simulate the influence of gas bubbling in a tundish on inclusion separation. Experiments have been conducted to examine the influence of a floating particle sink (simulated slag layer), a flow pattern modifying impact pad, and a gas diffusing bubbler on particle separation efficiencies. Particle separation experiments also examined the influence of gas flow rate, tundish residence time, particle size and bubble size. The physical modeling experimental results confirmed that particle separation by gas bubbling in a tundish can be an efficient method for enhancing inclusion flotation. It was also confirmed that relatively small bubbles (<1mm in diameter) are required for maximum particle separation efficiency.

2.0 LITERATURE REVIEW

There has been only a limited amount of research conducted on the influence of inert gas bubbling in the tundish of a continuous casting machine on inclusion removal from liquid steel, and some models have been developed [3-6]. As well, some plant trials have been conducted which indicate the beneficial potential of tundish bubbling [7]. Recently, Zhang and Taniguchi [8] have reviewed the fundamentals of inclusion removal from liquid steel by attachment to rising bubbles. Zhang and Taniguchi's study provides an overview of the mechanisms of bubble/inclusion interaction and a model for inclusion removal by bubbling in a batch process such as ladle stirring.

An important mechanism for inclusion elimination from liquid steel is that of simple flotation, whereby the particle is separated if it rises as the result of its buoyancy to contact the slag and is then absorbed by the slag. However, the efficiency of inclusion removal by simple flotation in a tundish is generally limited by the residence time of liquid metal as it flows through a tundish and the rise velocity of the buoyant particles. The rise velocity of a particle is a function of its size, smaller particles are harder to remove. Gas bubbles have higher rise velocities than inclusions as a result of being less dense and typically larger in size. Thus, particle/bubble attachment is an important topic in the enhancement of inclusion separation in a tundish.

2.1 Particle/Bubble Collision and Attachment

Fig. 2, (adapted from Nguyen et al. [9]) shows the angular relations between a rising bubble in a liquid medium and approaching particles. The two important angles illustrated in this figure are firstly the critical angle of attachment (θ_A), which is defined as the polar angle beyond which no adhesion between the bubble and particle occurs, and secondly the collision angle (θ_C), which is defined as the polar angle, not exceeding 90° , beyond which no collision occurs between the bubble and particle. For example as illustrated in Fig. 2, particle 1 having an approach angle less than θ_A will collide and attach to the bubble, while particle 2 having an approach angle less than θ_C but greater than θ_A will collide with the bubble but not attach, and particle 3 having an approach angle greater than θ_C will not collide with the bubble. Particles with approach angles less than θ_C will collide with the bubble and slide along the bubble surface. The induction time is the sliding time required to achieve stable three-phase (particle/liquid/gas) contact (TPC) and particle attachment. By definition, particles having approach angles less than θ_A will both collide with the bubble and have sufficient contact time to become attached to the bubble. Particles having approach angles greater than θ_A but less than θ_C will collide with the particle but have insufficient sliding time to become attached.

Liquid flow around the bubble may be predicted by potential flow or Stokes flow models, or a combination of both, to be fore-and-aft symmetric [9]. However based upon semi-analytical results of the Navier-Stokes equations, Nguyen found that the liquid flow

around a bubble at intermediate bubble Reynolds number is fore-and-aft asymmetric, and from this Nguyen calculated the particle/bubble attachment probability as [10]:

$$P_{at} = \frac{X+C+Y \cos \theta_A}{X+C+Y \cos \theta_C} \left(\frac{\sin \theta_A}{\sin \theta_C} \right)^2 \quad (1)$$

The constants C , X , and Y are dimensionless parameters. These parameters are a function of particle size, bubble size, and bubble Reynolds number ($0 < Re_b < 400$) and their defining equations are given in Appendix 9.4. It is important to note that the probability of attachment (P_{at}) does not include the probability of collision, as will be discussed subsequently. If the first part of Equation (1) is unity, the equation reduces to the Dobby and Finch [11] attachment efficiency model:

$$P_{at} = \left(\frac{\sin \theta_A}{\sin \theta_C} \right)^2 \quad (2)$$

Both Nguyen and Kmet [12] and Dobby and Finch [11] have developed formulas for the collision angle as a function of the bubble Reynolds number. The equation proposed by Nguyen and Kmet is:

$$\theta_C = \arccos(D) \quad (3)$$

where D is a dimensionless parameter. D is a function of the bubble Reynolds number valid for $0 < Re_b < 400$, and the equation defining D is given in Appendix 9.4. In any case to predict the attachment probability by Equation (1), it is necessary to determine the critical angles (θ_A, θ_C). But, there exists a lack of experimental data or modeling to predict θ_A . Thus in order to predict the attachment probability, Nguyen's sliding time model given below by Equation (4), must be utilized [10].

$$t_s = \frac{d_p + d_B}{2u_B(1-B^2)A} \ln \left\{ \frac{\tan \frac{\theta_m}{2} \left[\operatorname{cosec} \theta_m + B \cot \theta_m \right]^B}{\tan \frac{\theta_o}{2} \left[\operatorname{cosec} \theta_o + B \cot \theta_o \right]} \right\} \quad (4)$$

where A and B are dimensionless parameters. These parameters are a function of bubble Reynolds number, and their defining equations are given in Appendix 9.4. Angles θ_o and θ_m are polar angles at the beginning and the end of sliding contact interaction, respectively. When θ_o equals the critical angle of attachment (θ_A), particles that begin sliding at this critical polar angle are called particles of critical attachment and the sliding time of the particles of critical attachment can be equated to the induction time, t_i .

Nguyen et al. [9] have shown that the collision angle (θ_C) corresponds to the maximum angle of contact (θ_m). Consequently, the induction time can be predicted using the sliding time model for the particles of critical attachment by substituting θ_A and θ_C for θ_o and θ_m respectively on the right hand side of Equation (4) and t_i for t_s on the left hand side. Then we obtain:

$$t_i = \frac{d_p + d_B}{2u_B(1-B^2)A} \ln \left\{ \frac{\tan \frac{\theta_C}{2} \left[\operatorname{cosec} \theta_C + B \cot \theta_C \right]^B}{\tan \frac{\theta_A}{2} \left[\operatorname{cosec} \theta_A + B \cot \theta_A \right]} \right\} \quad (5)$$

Now by combining Equations (2), (3), and (5), the unknowns (θ_A, θ_C) can be eliminated and an expression relating the induction time and attachment probability is produced:

$$t_i = \frac{d_p + d_B}{2u_B(1-B^2)A} \ln \left\{ \frac{\frac{1}{\sqrt{P_{at}}} + \sqrt{\frac{1}{P_{at}} + D^2 - 1}}{\left(\frac{1}{\sqrt{P_{at}}} + B \cdot \sqrt{\frac{1}{P_{at}} + D^2 - 1} \right)^B} \cdot \frac{(1+BD)^B}{1+D}} \right\} \quad (6)$$

Equation (6) has been shown by Nguyen et al. [6] to be valid for both fore-and-aft symmetric and fore-and-aft asymmetric flow around bubbles with Reynolds numbers in the range $Re_b < 400$. If the induction time is known, the attachment probability can be found from Equation (6).

The film drainage time (t_{FC}) was determined by Schulze [13] to be:

$$t_{FC} = \frac{3\mu}{64} \frac{\alpha^2}{k\sigma h_{Cr}^2} d_p^3 \quad (7)$$

where k is a constant, and equals four for a completely unretarded gas bubble (i.e. one with a mobile surface) [8].

The induction time is the time needed for drainage between a bubble and a particle to the rupture of the film and the formation of a stable TPC line. Zhang and Taniguchi [8] ignored the rupture time and time for formation of a stable TPC line and equated the induction time to the film drainage time during collision (t_{FC}). In which case:

$$t_i = t_{FC} \quad (8)$$

The overall probability of particles being collected by bubbles is the product of the collision probability (P_c), the attachment probability (P_{at}), and one minus the detachment

probability $(1 - P_{det})$ [6]. The detachment probability is generally not considered when solving for the overall probability [9,11], which is equivalent to assuming that the detachment probability is zero, and as a result the particle collection probability is given by:

$$P = P_c \cdot P_{at} \quad (9)$$

Several researchers have derived models for the collision probability, the most recent of which has been obtained from a semi-analytical solution of the Navier-Stokes equations by Nguyen et al. [9,12]:

$$P_c = \frac{2u_B D}{9(u_B + u_p)Y} \left(\frac{d_p}{d_B}\right)^2 \left[\sqrt{(X+C)^2 + 3Y^2} + 2(X+C) \right]^2 \quad (10)$$

where X and Y are dimensionless parameters. These parameters are a function of bubble Reynolds number, and their defining equations are given in Appendix 9.4.

2.2 Bubble Rise Velocity

Zhang and Taniguchi [8] reviewed several models for terminal bubble rise velocity and found that the overall agreement between the models was not good. However, the equation proposed by Davies and Taylor [14] for spherical cap bubbles of equivalent bubble diameter greater than 6mm can be used to calculate the rise velocity as follows:

$$u_B = 1.02 \left(\frac{gd_B}{2} \right)^{1/2} \quad (11)$$

For small spherical bubbles ($\ll 1$ mm), Stokes law can be used to predict the rise velocity:

$$u_B = \frac{d_B^2}{18\mu} g(\rho_L - \rho_G) \quad (12)$$

For bubble sizes greater than 1mm, the Stokes law equation predicts bubble rise velocities in water that are higher than those measured experimentally [15]. For bubbles in the size range of 1 to 6mm, the bubble rise velocity declines until stable spherical cap shaped bubbles are formed. The rise velocity of large spherical-cap bubbles in water has not been found to exceed the rise velocity of bubbles around 1mm in diameter until the equivalent diameter of the spherical-cap bubbles exceeds 30 to 40 mm. For bubble diameters between 0.5 to 6mm, the Davie and Taylor relation (equation 11) provides the best estimate of bubble rise velocity in the absence of experimental data.

2.3 Capillary Effects On Inclusion Separation

Hongbin et al. [16] used a confocal scanning laser microscope (CSLM) and an infrared image furnace to carry out *in-situ* real-time observation of the collision and agglomeration behaviour of inclusion particles on the surface of steel melts at high temperatures. Shibata et al. [17] found that alumina inclusions exhibited a long-range attraction to each other, spanning a few tens of μm . This attractive force was found to increase with the size of the particles. Particles at the gas-steel interface were observed to attract each other in fractions of a second and then agglomerate into larger particles. This attractive force was attributed to capillarity. These studies [16,17] indicate that capillary forces may have an important influence on inclusion separation. Once an inclusion has become attached to a bubble, the capillary effect should increase the probability that other

particles colliding with the bubble then adhere. This effect would become greater with increasing agglomerate size. Also once inclusions have been floated to the surface of the tundish, they should quickly agglomerate, making it more difficult for particles to be re-entrained into the liquid steel.

3.0 MATHEMATICAL MODEL OF TUNDISH BUBBLING

3.1 Development of Mathematical Model

The collision probability calculated using Equation (10), as a function of bubble and particle size, is presented in Fig. 3, where the parameters C , D , X and Y are calculated using the relations (presented in Appendix 9.4) as given by Nguyen et al. [9], and where u_B and u_P are calculated using equations (11) and (12) respectively. From this figure, it is noted that the collision probability is predicted to be less than 15% for bubbles greater than 1mm and particles smaller than 100 microns. Collision probability is found to increase with decreasing bubble size and increasing particle size.

As discussed previously, P_{at} can be estimated using Equations (6), (7) and (8). Fig. 4 presents the calculated product of attachment and collision probabilities and illustrates that particle collection efficiency increases as bubble size decreases. The attachment probability is generally greater than 80% and thus the particle collection probability (P) is dominated by the collision probability as seen when comparing Figs. 3 and 4. The results of these calculations for bubble sizes greater than ~3mm are questionable, since for bubbles > 3mm diameter the bubble Reynolds number exceeds 400, beyond which the equations are no longer valid. Although according to these calculations it is desirable to produce the smallest bubble size possible, since collection probability increases exponentially with decreasing bubble size, it should be noted that very tiny bubbles becoming entrained in the tundish outflow might not separate from the liquid metal in the

tundish. Thus, some minimal bubble size with sufficient rise velocity to assure bubble float-out would be optimal for inclusion separation in a tundish.

In a manner similar to that of the batch model derived by Zhang and Taniguchi [8], a simple model describing inclusion removal by gas bubbling in the channel of a continuously flowing tundish can be derived. This model is illustrated schematically in Fig. 5. The simplifying assumptions of this tundish bubbling model include the following:

- All bubbles are of identical size, and are uniformly distributed in the ‘bubbly’ region of the tundish. Thus, bubble/bubble interactions are ignored.
- Inclusion particles have a fixed size and are also uniformly distributed in the liquid steel. Thus, the particles are assumed to be too small to affect bubble motion and particle/particle collision and agglomeration effects are ignored.
- Particles are removed by attachment to rising bubbles and subsequent transport of the attached particles to the floating slag layer where the particles are collected and the gas escapes. Other removal mechanisms, such as simple particle flotation and collision/attachment with other collecting surfaces (such as the tundish walls) are ignored. Also, re-entrainment of particles into the liquid by turbulence at the slag/metal interface is ignored.
- The bubble size is independent of the gas flow rate, which implies that some special gas injection apparatus is assumed to produce a fixed bubble size.
- The liquid metal carrying the inclusion particles has a plug-type flow through the bubbly region of the tundish and thus the residence time of the liquid steel in the

bubbly region of the tundish is simply the volume fraction of the bubbly region times the overall residence time of liquid metal in the tundish.

In this model, the number of collecting collisions with inclusions per bubble is given by:

$$N_{CC} = V_{BC} \cdot n \cdot P = \frac{\pi}{4} d_B^2 H n P \quad (13)$$

where the particle collection probability (P) has previously been defined by Equation (9).

The number of bubbles supplied to the liquid steel per unit time per unit of bubbly volume is:

$$N_B = \frac{q_G A_{BS}}{V_B} \cdot \frac{T_F}{T_o} \cdot \frac{1}{V \frac{L_B}{L}} = \frac{6q_G T_F}{\pi d_B^3 T_o H} \quad (14)$$

The total number of collecting collisions per unit time per unit of bubbly volume is:

$$N_T = N_{CC} \cdot N_B = \frac{3q_G P T_F}{2d_B T_o} \cdot n = K \cdot n \quad (15)$$

where the rate constant (K) is given by:

$$K = \frac{3q_G P T_F}{2d_B T_o} \quad (16)$$

T_F is taken as 1800 K in this study and T_o is the temperature of the gas, which is assumed to be 300 K. The inclusion concentration (n) is a function of the residence time of the liquid in the bubbly region, thus the rate of inclusion removal can then be represented by Equation (17):

$$-\frac{dn}{dt} = N_T = K \cdot n \quad (17)$$

The residence time of liquid in the bubbly region of the tundish (τ) is given by the product of the mean residence time of liquid in the overall tundish by the volume fraction of the bubbly region. Thus:

$$\tau = \tau_T \cdot \frac{L_B}{L} \quad (18)$$

Integration of Equation (19) from $t = 0$ to τ and $n = n_o$ to n provides the relation:

$$n = n_o e^{-K\tau} \quad (19)$$

Since the removal efficiency of inclusions (ε) can be represented by:

$$\varepsilon = \frac{n_o - n}{n_o} \cdot 100 \quad (20)$$

Combining Equations (19) and (20) yields the following relation which expresses the inclusion removal efficiency as a function of the rate constant (K) and the residence time of liquid steel in the bubbly region of the tundish (τ):

$$\varepsilon = (1 - e^{-K\tau}) \cdot 100 \quad (21)$$

Figs. 6 and 7 illustrate the results of calculations using the above model of inclusion separation from liquid steel in a tundish. Fig. 6 shows the influence of bubble size (d_B) and volume fraction of the bubbly region (L_B/L) on the removal efficiency of inclusion particles by gas bubbling in a tundish. This figure indicates that a bubble size less than 1mm is required to achieve an ideal perfect separation of inclusions 20 μ m in diameter or smaller. For larger particles on the order of 100 μ m diameter, bubbles of 5mm diameter and a bubbly volume fraction greater than 0.4 can still achieve a near perfect separation of the inclusions. Fig. 7 illustrates that for bubbles of 1mm diameter, high inclusion removal efficiencies are largely independent of bubbly volume fraction and tundish

residence time in the practical range of 240 to 720s. However, for larger bubble sizes on the order of 5mm in diameter, the influence of residence time and bubbly volume fraction cannot be neglected. Higher residence time and larger bubbly volume fraction increase inclusion separation.

3.2 Interpretation of Mathematical Model Results

3.2.1 Minimum Bubble Size

It is possible that there is some bubble size or bubble rise velocity below which bubbles may not escape the liquid in the tundish as a result of being entrained in the exiting flow. To avoid such entrainment, the bubble rise velocity must exceed some minimum that is determined by the velocity of the liquid flow and the proximity of the bubble source to the tundish outlet.

The minimum bubble size for bubble escape can be estimated knowing the mean liquid velocity toward the outlet (u_L), the depth of the tundish (H), and the minimum distance between the bubble source block and the tundish outlet (L_{min}). Equating the time for a bubble to rise and escape ($H/u_{B,min}$) to the time for the bubbly liquid to reach the outlet (L_{min}/u_L) yields the following relation for the minimum bubble rise velocity:

$$u_{B,min} = \frac{H \cdot u_L}{L_{min}} \quad (22)$$

For $H = 1\text{m}$, and $L_{min} = 0.25\text{m}$ and taking a tundish residence time (τ_T) of 480s, the mean liquid velocity (u_L) typically is on the order of 0.0085 m/s. Therefore $u_{B,min}$ is

approximately 0.033 m/s, which according to Stokes law corresponds to a minimum bubble size of 0.25mm to avoid bubble entrainment in the outlet flow. Thus, a bubble size on the order of 1mm provide a high probability for bubble escape from the tundish, while as previously discussed, such a bubble size can theoretically provide a high efficiency of inclusion removal.

3.2.2 Control of Bubble Size

Several factors are important in control of bubble size. These include gas flow rate per bubble orifice, orifice size and shape, surface tension and viscosity of the liquid metal, wetting angle of the porous medium with liquid steel, and stirring or turbulence intensity in the liquid. The influence and interrelationship of each of these factors is very complex. For example, it is expected that bubble diameter will increase as gas flow rate increases, but this is dependent on the bubble orifice Reynolds number.

$$N_{Re,O} = \frac{u_b d_o \rho_G}{\mu} = \frac{4Q\rho_G}{d_o \mu} \quad (23)$$

where d_o is the diameter of a single orifice which is feeding gas into the liquid. At a very low gas flow rate per orifice, the bubble size may be simply determined by a balance between surface tension and buoyancy force, in which case the bubble size is independent of gas flow rate. This balance yields the following equation that is valid for $N_{Re,O} < 500$ [15]:

$$d_B = \left[\frac{6d_o\sigma}{g(\rho_L - \rho_G)} \right]^{1/3} \quad (24)$$

Whereas, for very high bubble orifice Reynolds numbers, the bubble size may totally depend on the gas flow rate. For example, for $N_{Re,O} > 5000$ in aqueous systems, it has been found that [18]:

$$d_B = \frac{1.3Q^{6/5}}{g^{3/5}} \quad (25)$$

When the liquid wets the orifice material, the bubble forms at the perimeter of the orifice as shown on the left side of Fig. 8 [18]. If the liquid does not wet the orifice material, the bubble will expand across the surface of the orifice material as shown on the right hand side of Fig. 8. As a consequence, for the case of low $N_{Re,O}$ and a single non-wetted orifice of known outer diameter, the bubble size on detachment would be given by [18]:

$$d_B = \left[\frac{6d_{n,o}\sigma}{g(\rho_L - \rho_G)} \right]^{1/3} \quad (26)$$

where, $d_{n,o}$ is the outer diameter of the orifice block. Thus for porous material that is not wetted by liquid metal, bubbles may expand across the porous material. This could have two complicating effects on bubble size control; firstly, multiple orifices may feed a forming bubble, and secondly bubbles may coalesce on the surface of the porous material before detachment. These effects have been observed in a study by Wang et al. [19] who used a water model and a hot (liquid iron) model to simulate gas injection through a porous block into liquid steel. In the water modeling it was observed that small bubbles

were formed when the porous material was wetted. However, coating the porous material with paraffin wax to render the substrate non-wetted resulted in the coalescence of the bubbles into large sheets of gas and this was attributed to the spreading of the gas along the solid/liquid interface and the feeding of the gas sheet by multiple pores. This effect was confirmed in the hot modeling where a non-wetted porous refractory block was used.

The above discussion is problematic for the current technology for the design and manufacture of bubble source blocks for the enhancement of inclusion removal in a tundish. The formation of bubbles $< 3\text{mm}$ is very difficult if not impossible with the porous plugs currently used in industry, as they are generally fabricated from porous materials that are nonwetted by molten metal [20]. Presumably, high stirring or turbulence intensity in the liquid phase would favour the formation of small bubbles however, Sahai and Guthrie [21] compared the results of several researchers and found that the normal injection of gas into liquid steel is accompanied by the formation of very large bubbles that are invariably of the spherical cap variety owing to the high surface tensions of liquid metals and the non-wetting characteristics of the refractory materials used for bubbling blocks. Consequently, the particle collection efficiency would be relatively low when using the common, nonwetted porous plug block to remove inclusions from the liquid steel in a tundish. This disadvantage has promoted research on nozzles with novel shapes.

3.2.3 Novel Designs For Non-Wetted Slot Nozzles

Okumura et al. [20] studied the bubble formation from nonwetted slot nozzles in water and mercury. Teflon plates were used in the water model for fabrication of the slot nozzle, and an acrylic resin slot nozzle was used for the mercury model. Okumura et al. [20] found that for both the water and mercury experiments, gas bubbles were formed along the slot at discrete locations, which they referred to as “bubble sources”. The bubbling behaviour was grouped into two distinct regimes, I and II, which depend on gas flow rate. For low gas flow rates the bubbles sources were attributed to the existence of Rayleigh-Taylor instability on the slot mouth. The number of bubble sources increased with increased gas flow rate (regime I), until a critical point at which bubbles growing neighbouring sources touched. Beyond this critical point, the number of bubble sources decreased with increasing gas flow rate (regime II), until a continuous blanket of gas formed along the slot mouth. The use of a slot nozzle was noted to produce smaller bubbles and a wider bubble plume than that produced from a porous plug. It was also noted that the number of bubble sources was less than observed for gas injection from a wetted slot nozzle [20].

Traditionally, wetted materials have not been widely used in fabrication of porous plugs since steel penetration into the pores is an issue for high liquid steel head pressures. The tundish flow channel may be a good application for wetted refractory materials since the head pressure of steel is significantly lower than that of a ladle. Wetted refractory materials generally have a much smaller pore size and may not exhibit the same

coalescence of bubbles at the nozzle surface as has been observed with nonwetted materials.

3.3 Discussion of Mathematical Model Results

The probability of particle/bubble attachment (P_{at}) is the product of the probabilities of the three fundamental steps of this process, including film thinning, film rupture and TPCL expansion to stability. However, only the probability of film thinning is calculable by any known method and it has been suggested that the probability of the last two steps can be assumed to be unity, in which case the probability of film thinning can be equated to the probability of particle/bubble attachment. Such an analysis leads to the following findings: (i) P_{at} increases with decreasing particle size, (ii) P_{at} increases with increasing bubble size, and (iii) P_{at} is greater than 80 percent. However, a particle must first collide with a bubble before the attachment process can begin. Thus, particle collection probability (P) is the product of P_{at} and the collision probability (P_C). Since the collision probability is generally much lower than the attachment probability, the overall collection probability is controlled by the collision probability. A semi-analytical solution of the Navier-Stokes equations by Nguyen et al. [9, 10] has been used to estimate collision probabilities. This analysis shows that the collection probability (P) increases with decreasing bubble size and increases with increasing particle size.

A simple math model has been developed to describe the efficiency of inclusion removal from liquid metal flowing through a tundish as the result of bubbling. This

model predicts that inclusion removal efficiency (ε) is maximized as bubble size is decreased. This prediction is the result of inclusion removal efficiency being strongly affected by the particle collection probability (P). The current technology of bubbling blocks for use in steelmaking vessels such as a tundish may not be capable of producing bubbles of the small size necessary to maximize inclusion removal efficiency, since such blocks are generally fabricated from material that is not wetted by liquid steel. As a result, other factors must be taken into consideration in the maximization of inclusion removal efficiency. For relatively large bubble sizes (e.g. $>3\text{mm}$) the effect of tundish residence time (τ_T) and the bubbly volume fraction (L_B/L) are substantial. Increasing the area over which bubbles are introduced in to the tundish, i.e. increasing the bubbly volume fraction (L_B/L) can significantly increase inclusion removal efficiencies. As well, longer residence times of the liquid steel in the tundish promote enhanced removal efficiencies by allowing greater time of contact in the bubbly region and allowing inclusions a longer time to be removed by simple flotation. The model indicates that for high removal efficiencies ($>80\%$) of inclusions less than 60 microns in size, bubbles less than 3mm in diameter should be used. Thus, the development of new technologies for the introduction of tiny gas bubbles into liquid steel is expected to be very helpful to the application of tundish bubbling as a means for inclusion removal enhancement.

4.0 EXPERIMENTAL METHOD - PHYSICAL MODELING

4.1 Apparatus

Experiments were performed in a 1/3-scale model of a typical single-strand tundish. Single-strand tundishes are in common use in the steel industry and a single-strand model is less complex as compared to one with multiple strands. Since the general shape of single-strand tundishes does not vary greatly throughout the industry as compared to multiple strand tundishes, the configuration chosen in these experiments is representative of a large number of operating casting machines.

The tundish model was fabricated from clear acrylic with internal dimensions shown in Fig. 9. A large vessel was utilized as the ladle and was positioned overtop of the tundish as seen in Fig.10. Water was continuously fed into the ladle by a hose to maintain a constant level. A two-inch gate valve was employed to control flow into the tundish and a one-inch I.D. steel pipe was used for a ladle shroud, all pertinent dimensions are provided in Fig. 10. Since it is common in the industrial practice to use an impact pad in the tundish to dissipate the momentum of the inlet stream, an impact pad as illustrated in Fig. 10 was utilized in some experiments as will be explained subsequently. Also, as will be discussed later, a ‘vortex killer’ was used in all experiments to prevent vortexing of the outlet flow. The outlet flow rate from the model was controlled using an orifice drilled to a specific size for a given flow rate and tundish head, and the calculated flow rate from the model was occasionally checked against the

achieved rate by recording the time to fill a known volume. The measured (i.e. achieved) rates were always $\pm 2\%$ of the predicted (calculated) rates.

Particles were injected into the ladle shroud with a 60cc wide-nose syringe. Particles that did not separate from the liquid in the tundish were collected from the outlet stream of the tundish with a 400-mesh sieve (38 μm opening). This sieve was equipped with a vertically extended upward wall to prevent loss of particles by splashing. The 400-mesh screen provided a good collector, as water could easily drain through it at the flow rates of the experiments, while at the same time particles could not pass through the mesh, as particle size was always greater than 53 μm .

The housing of the tundish diffuser block was also fabricated from clear acrylic; dimensions of the block are given in Fig. 11. A porous block of alumina-graphite was bonded into the housing using five-minute epoxy. Air was fed into the bottom of the block through a copper pipe that screwed into the block and sealed the block to the bottom of the tundish. Gas flow rate was controlled with a Matheson flowmeter (tube#603).

4.2 Experimental Approach

Physical modeling experiments were conducted using the apparatus described in Section 4.1 above once a suitable particulate material was found. The choice of particle used in the physical model is an important element in the proper simulation of the

separation behaviour of typical inclusions found in liquid steel (alumina or aluminate particles for example) and some difficulties were experienced in finding a suitable material for use in water. However, after much consideration it was decided to adopt linear low-density polyethylene (LLDPE) as the particulate material to be used in the model. Thus in the physical modeling experiments, water served as an analogue medium representing liquid steel and LLDPE particles served as an analogue for the solid inclusions found in liquid steel.

Hollow glass microspheres, with specific gravity of 0.37, were initially considered as an analogue material for use in the aqueous environment to represent inclusions in liquid steel. Although the density ratio of the microspheres to water was very similar as compared to that of alumina/liquid steel ($\rho_{\text{alumina}}/\rho_{\text{liq. Steel}} = 3.2/7.05 = 0.45$), it was found that the microspheres also had various disadvantages. The primary disadvantage of the glass microspheres was that they were extremely difficult to handle and sieve due to their very low specific gravity. Sieving was necessary in order to separate the particles into various size ranges so that the effect of particle size on separation efficiency could be examined. However, sieving of the glass microspheres proved to be a tortuous, inefficient and largely ineffective process. The results of preliminary tundish modeling flotation experiments with the glass microspheres were irreproducible, and this was attributed to difficulties of producing samples of particles with the same size distribution. Irreproducible particle separation behaviour of the microspheres may also have been the result of particle re-entrainment since there was no particle sink to receive them at the top free surface of the water in the tundish. Although the problem of re-entrainment of the

microspheres could perhaps be solved by the addition of a floating particle sink (i.e. an absorbing layer) on the free surface of the liquid in the tundish, no readily available, easy to use, floating medium that is immiscible in water was found that would readily accept the glass microspheres.

Eventually it was decided to test LLDPE particles, when it was discovered that LLDPE particles are absorbed by kerosene. Since kerosene also floats on and is immiscible in water, it makes an excellent medium to use as a sink for LLDPE particles in a water model. LLDPE is not wetted by water (contact angle ~ 105 degrees [22]) and thus the contact angle simulates the not-wetted characteristics of alumina inclusions in liquid steel. The ability of LLDPE to be absorbed by a floating kerosene layer and the high contact angle of the particles in water provide a good simulation of the steel system where inclusion particles are easily expelled from the liquid as the result of high contact angles and where inclusion particles are absorbed by the floating slag layer.

The as-received polyethylene particles (LLDPE) had a relatively large average particle size, and consequently only a small mass fraction was utilized once the desired size distributions were achieved. However, even though the recovered size fraction was small in extent, sieving of the LLDPE particles was far simpler as compared to the glass microspheres. LLDPE sieving was carried out using standard ASTM sieves to produce two size ranges of particles for experiments, +270/-200 mesh (53 to 75 μm) and +200/-160 mesh (75 to 106 μm).

With LLDPE particles in water, the specific gravity ratio of solid/liquid was far higher than that of alumina inclusions/liquid steel, given that the specific gravity of the LLDPE particles used was 0.92. Thus, dimensional analysis was performed to determine the relation between the simulated particle sizes and particle sizes in the system being modeled. This dimensional analysis is presented in the Appendix (Section 9.2). This analysis shows that the 53 to 75 μm size range represents 25 to 36 μm particles in the full-scale alumina/liquid steel system and that the 75 to 106 μm particle size range represents 36 to 51 μm in the full-scale system.

An ample amount (>200g) of both particle size ranges (53 to 75 μm and 75 to 106 μm) were sieved to provide sufficient particles to complete all of the experiments. The large quantities of particles were accumulated in order to assure consistency of the particle size distributions used throughout all the experiments, so as to avoid the inconsistencies that occurred when using the glass microspheres. A 6.00g quantity of particles was used for each experiment. This quantity fit the capacity of the injection syringe and provided reasonable simulation of particle concentration in liquid steel (see Appendix, Section 9.3)

In preparation for an experiment, a particle collector (i.e. a 400 mesh sieve with upward extended wall) was completely dried and then weighed on an Adams Equipment ACG-600H balance (Max Capacity=600g, resolution = 0.01g) to provide a tare weight of the particle collector. With the given tundish furniture set-up, steady state water flow was achieved in the tundish model system and the given flow rate of air, for gas bubbling, was set on the gas flowmeter. A 6.00g sample of particles was then weighed out on the

balance and this sample was placed into a 60cc syringe from which the plunger had been removed. The remaining volume of the syringe was filled with isopropyl alcohol. This was done in order to create an injectable particle slurry, since the LLDPE particles created a homogeneous mixture with the alcohol. Just prior to the start of the experiment the particle collector was placed into the exiting stream.

At time $t = 0$, a timer was started and the particle sample was injected with the syringe. Once the plunger of the syringe was fully depressed (at approx. $t = 5s$), the plunger was then cycled back and forth 3 times in order to ensure that the entire sample was injected into the system. The particle injection process was complete in less than 20 seconds. Particles were then collected for three tundish residence times ($3\tau_T$) at which point all particles had either separated from the tundish bath or had been collected in the particle collector. At the conclusion of the experiment, the particle collector was removed from the exit stream and placed under a heat lamp (for approximately 24 hours) until completely dry. Once dry, the particle collector containing the collected particles was weighed. The mass of the collected particles was easily determined by subtracting the tare weight of the collector.

5.0 TUNDISH RTD MEASUREMENTS

In order to determine the influence of the impact pad and bubbler on the overall flow behaviour in the tundish, residence time distribution (RTD) experiments were conducted using the water modeling apparatus. In the RTD experiments, a highly concentrated salt solution (250g salt/litre of water) was injected into the ladle shroud, and salt concentration in the outlet stream was continuously measured with an electrical conductivity probe. Concentration vs. time data were acquired by computer and subsequently converted into normalized residence time distribution curves.

Figs. 12 to 14 present the measured RTD curves. Initially a baseline RTD curve with no furniture in the tundish (i.e. no impact pad, no dam, and no bubbler) was determined. The influence of the presence of an impact pad and dam in the tundish on the RTD curve was then examined. The dam was used in conjunction with the impact pad to represent the presence of a bubbling block in the tundish but without gas injection. In further tests, the influence of tundish bubbling on RTD was examined with and without the impact pad.

Fig. 12 shows that the minimum residence time (short-circuit time) is doubled (from 0.1 to 0.2 normalized time units) using the impact pad and dam as compared to the baseline with no tundish furniture. This increase in short-circuit time should provide an increased opportunity for the separation of relatively large inclusion particles by simple flotation. Also as shown in Fig. 12, the peak height of the RTD curve with the impact

pad and dam is much higher than was measured in the baseline configuration (no impact pad, no dam, no bubbling). This higher peak in normalized concentration occurs at nearly the equivalent time as the peak in the baseline test and this effect means that the flotation of relatively small size inclusions may not be beneficially affected by the presence of the tundish furniture.

Fig. 13 compares the RTD curve for a tundish with bubbling at a rate of 0.5 litre/min to the RTD curve of the baseline tundish. These curves are fairly similar in shape and the minimum residence times are identical, but the lower peak concentration height for the bubbling curve indicates a slightly more mixed flow nature in the tundish with bubbling. The peak concentration time is somewhat higher with bubbling as compared to the baseline, which indicates a slightly better RTD for inclusion separation. However, overall there is little difference between the RTD curves to indicate that the bubbling alters the RTD in a way that would significantly increase particle separation efficiency.

Fig. 14 shows the RTD curve for a tundish equipped with an impact pad and a bubbler as compared to the baseline RTD curve. In this case there is a benefit of increased minimum residence time and a shifting of the peak concentration time to the right when using the impact pad and bubbler. These alterations to the RTD when using both an impact pad and bubbler as compared to the baseline tundish indicate somewhat improved potential for inclusion float-out with impact pad and bubbler.

6.0 PARTICLE SEPARATION RESULTS

6.1 Initial Physical Modeling

A significant observation was made during one of the initial experiments in which bubbling was used in the tundish. A dimple was occasionally observed to form on the liquid bath above the tundish outlet and the outlet stream was swirling and ropy in nature whenever the dimple was seen, whereas in the absence of the dimple the outlet stream was smooth and laminar. These observations indicated that a draining vortex could sometimes occur during an experiment even though the overall flow was at steady state. Later, comparison of the results of this experiment with another identical experiment during which vortexing was not observed showed a significant increase (~30%) in the mass of particles collected when vortexing occurred. At this point it was decided that a ‘vortex-killer’ should be inserted into the tundish for all subsequent experiments so as to prevent occasional and/or unobserved vortexing that would affect the reliability and reproducibility of particle separation results. The ‘vortex-killer’ was a thin wall that protruded from the tundish wall as shown in Fig. 10. The interference of the protruding wall was found to deter the formation of a steady rotational flow component that can lead to vortexing above the outlet. With the ‘vortex-killer’ installed, no vortexing was observed in any subsequent experiments.

6.2 Primary Matrix of Physical Modeling Experiments

In order to understand the relative influence of bubbling on particle separation in a tundish compared to other factors, a primary experimental matrix was developed. Since, the addition of an impact pad to the tundish has generally been accepted as a means to increase inclusion flotation, the primary experimental matrix included tests with and without an impact pad. Also, tundishes are generally covered in a slag, which acts as a particle absorbing sink, thus it may be assumed that in the real system once an inclusion reaches the slag layer, re-entrainment of the inclusion is not an issue. In order to ascertain if re-entrainment could be an issue in the model, it was desired to put a slag-like particle sink on the liquid surface of the tundish. Kerosene was chosen as the particle sink since it floats on water and LLDPE particles dissolve into it. The presence of a kerosene slag layer, an impact pad, and tundish bubbling were chosen as the three key parameters for investigation in the primary experimental matrix and this matrix is presented in Table 1.

Parameters	Experiment Type							
	Baseline		Impact Pad		Bubbling		Bubbling & Impact Pad	
Particle Sink	No	Yes	No	Yes	No	Yes	No	Yes
Impact Pad	No	No	Yes	Yes	No	No	Yes	Yes
Bubbling	No	No	No	No	Yes	Yes	Yes	Yes

For all tests in the primary matrix, the water throughput of the tundish was 27 litre/min (providing a simulated liquid steel throughput of 3 ton/min at 1/3rd scale according to a Froude number criterion, see Appendix, Section 9.1). The 75 to 106µm particle size distribution was used, and when bubbling was induced at gas injection rate

of 0.4 litre/min was applied to the same bubbling block for all experiments. All experiments were repeated three times to assure reproducibility and the average particle separation of the three tests is reported. Separation efficiency is defined as:

$$\text{Separation Efficiency} = \left(1 - \frac{\text{wt.recovered @ outlet}}{\text{wt.injected}} \right) \cdot 100\%$$

As mentioned previously a ‘vortex-killer’ was used in all experiments. The results of the primary experimental matrix are presented in the bar chart of Fig. 15 and these results are discussed below.

6.2.1 Baseline

The baseline tundish configuration included only a ‘vortex-killer’ and no other tundish furniture. For the baseline case, as shown in Fig. 15, the average particle separation efficiency was 45.1%. This low efficiency is attributed to the highly mixed flow pattern observed in the baseline tundish that maintained the majority of the particles entrained within the liquid bulk until they reached the outlet.

It was observed that some portion of the particles appeared on the free surface of the tundish bath within the first 30 seconds after particle injection and agglomerations of these particles were readily visible on the meniscus. Other portions of the particles were observed to be entrained within the liquid flow in large-scale eddies that extended throughout the entire tundish. Entrained particles were clearly visible, although their numbers were declining, throughout the bath in the tundish until about 2.5 tundish residence times (~11min) had elapsed. It was visually observed that the majority of

particles collected at the exit stream accumulated during the first residence time (i.e. when normalized time ≤ 1).

When experiments were conducted with the kerosene particle sink, particles reaching the meniscus were quickly and completely dissolved, disappearing into the kerosene layer once they reached the water/kerosene interface. The addition of the particle sink (kerosene layer) to the bare tundish was found to increase particle separation efficiency an additional 1.8%. As already noted, flow in the baseline tundish was of a highly mixed nature, particularly in the impact region where flow enters the tundish. In the impact region, flow from the ladle shroud flows up the adjacent back and side walls creating large eddies that may have been capable of re-entraining some particles from the meniscus. With the particle sink on the meniscus, the re-entrainment probability of particles should be greatly reduced as the result of the fast rate of particle absorption by the sink. Thus the 1.8% increase in separation efficiency with the kerosene layer is attributed to the reduction or elimination of particle re-entrainment.

6.2.2 Impact Pad

The impact pad tundish configuration included an impact pad located under the ladle shroud as shown in Fig. 10 along with a vortex killer. With the impact pad inserted in the system, the average particle separation efficiency was 65%. This is a significant improvement as compared to the baseline case. This improvement in separation efficiency appeared to be related to certain beneficial modifications to the flow in the

tundish as induced by the impact pad. Flow in the impact zone was far less turbulent and the re-entraining flow pattern established in the baseline experiments was eliminated. Overall flow in the tundish was far more plug-like and the minimum residence time was increased as shown by the RTD results discussed previously in Section 5. A large portion of flow issuing from the impact pad is directed upward to the meniscus. The improved tundish flow behaviour may not only explain the increase in particle flotation efficiency, but may also explain why the addition of the kerosene particle sink showed little further improvement (0.7%) to the results with an impact pad. The tundish flow behaviour was far less turbulent and more plug-like in nature with the impact pad as compared to the baseline and this reduction in turbulence and enhanced plug flow reduced the particle re-entrainment probability.

6.2.3 Tundish Bubbling

In the bubbling tests of the primary experimental matrix, air was injected at a rate of 0.4 litre/min into the bubbling block that was positioned in the tundish along with a vortex killer. In these experiments, it was observed by photographic analysis that the bubbles produced by the gas diffuser block were in the range of 0.5 to 0.75 mm diameter before particle injection. The bubbly region took the form of a vertically rising plume consisting of many columns of individually distinguishable bubbles. However after particle injection, it was observed that the average bubble size decreased quickly and significantly once the particles began encountering the bubbling block, producing a

bubble plume that appeared as a milky wall of tiny bubbles. It appears that particle interaction with the bubble surfaces during bubble growth caused earlier separation of the bubbles from the block. Bubble size was reduced into the range of 0.20 to 0.30mm in diameter. As a result of this significant decrease in bubble size, the rise velocity of the bubbles decreased and the bubble column rose at an angle to the vertical as it was pushed laterally by the liquid flow along the tundish. After about 1.6 residence times, the bubble column returned from the milky cloud like appearance that was associated with particle/bubble interaction to the original clear columnar bubble plume with the larger bubble size. At this same time, the overall volume of the tundish was visually observed to be free of entrained particles.

As seen in Fig. 15, the use of the tundish bubbler increased the average particle separation efficiency to 85%, which is nearly twice the efficiency of the baseline case without bubbling. Since there was no considerable difference found in the RTD curves (see Fig. 13), this substantial increase in separation efficiency cannot be attributed to an enhanced rate of simple flotation, but must be generated by some other mechanism. Although, the rising bubbles carry flow upward in the bubble plume region, thereby bringing particles closer to the top surface where they may more readily separate by flotation, this rising flow is also accompanied by a strong sub-surface flow away from the plume. This sub-surface flow may then return particles from near the top surface back into the liquid bulk. Thus enhanced separation of particles by attachment to rising gas bubbles, in accordance with the principles previously discussed in Section 2.1, should be considered as the principal mechanism accounting for the measured increase in

separation efficiency. The change in the appearance of the bubble plume as illustrated in Fig. 16, is direct evidence of interaction between the particles and the gas bubbles.

Particles were observed being carried upward within the rising bubble column and spreading outward from the plume on the liquid surface. The liquid surface above the bubble plume lightly bubbled and spread outward as the bubbles burst upon reaching the surface. Particles on the liquid surface surrounding the bubbling plume combined into increasing large floating agglomerations. A portion of the particles that did not reach the meniscus directly above the bubbler were carried along in the strong sub-surface flow underneath the meniscus until they either floated to the surface or were again entrained into the bulk flow. In this way, a large-scale re-circulating eddy was formed on the inlet end of the tundish between the ladle shroud and the bubbler as illustrated in Fig. 17. This re-circulation may promote particle separation, as particles entrained in this eddy would encounter the bubbly region numerous times and therefore have multiple opportunities for bubble attachment and separation.

It was found that the addition of a kerosene particle sink had little effect on the particle separation efficiency with gas bubbling. Although it was initially felt that any increase in sub-surface flow generated by the bubbling could increase the re-entrainment of particles, this concept was not supported by the experimental results. Adhesion between the floated particles and the water surface as the result of the high particle/liquid contact angle apparently provided sufficient force to retard any increase in re-entrainment with bubbling as compared to the baseline.

6.2.4 Impact Pad and Tundish Bubbling

Since experiments with an impact pad and with a bubbler each provided a significant increase in particle separation efficiency, it is logical to assume that installing both devices together in the tundish should increase particle separation as compared to either of these devices separately. Thus, experiments were conducted with both the gas diffuser and the impact pad in the tundish. However, the interesting result of these experiments was that using both the impact pad and gas bubbling only increased particle separation efficiency slightly as compared to gas bubbling alone. The separation efficiency with the bubbler and impact pad was 85.3% as compared to 84.8% with just the bubbler. These results indicate that the influence of the bubbler on particle separation overwhelms the influence of the impact pad. As discussed above, the bubbler produces a large recirculating eddy in the inlet end of the tundish, which enhances particle/bubble interaction and subsequent flotation.

The use of the kerosene layer provided a benefit of a further 4% increase in separation when using both impact pad and bubbler. The impact pad and bubbler tend to induce opposing flow patterns at the surface of the liquid bath between the two devices. This opposition appeared to promote turbulence in the regions where the flow patterns interacted. This turbulent interaction appeared to increase the potential for particle re-entrainment and therefore the use of the kerosene was helpful to retard this increased re-entrainment potential and as a result improve particle separation efficiency.

6.3 Comparison of Physical and Mathematical Modeling

The results of the primary experimental matrix proved that bubbling in the tundish has the highest particle removal efficiency of the factors tested. The influence of various parameters on the efficiency of particle separation by tundish bubbling was further analyzed in a second experimental matrix and compared to the predictions of the mathematical model presented in Section 3. The parameters analyzed were: gas (air) flow rate, particle size, tundish residence time, and gas bubble size.

6.3.1 Influence of Gas Flow Rate

In order to determine the influence of the gas injection rate, experiments were carried out with just the bubbler in the tundish (no kerosene) at volumetric gas flow rates of 0.2, 0.4, 0.8, 1.6, and 3.0 litre/min of air. A gas flow-rate of 3 litre/min was the highest flow-rate tested since this was the maximum the gas flow meter could measure. The results of these experiments are compared to the mathematical model predictions for various bubble sizes in Fig. 18.

As the gas flow-rate was increased up to 1.6 litre/min, bubble size was not observed to increase significantly, but the bubble plume became very dense with bubbles. As seen in Fig. 18, increasing the gas flow rate increased the particle separation efficiency. This is the expected result as predicted by the math model, since there will be an increased number of bubble/particle collisions as the number of bubbles in the bubbly portion of the

tundish is increased. Particle separation efficiency as a function of gas flow rate was found to follow a rule of diminishing returns as separation efficiency reached 95% at a gas flow-rate of 1.6 litre/min, whereas a further almost-doubling of the gas flow rate to 3 litre/min increased separation efficiency to only 96.5%. Thus a maximum or optimum gas injection rate for the bubbling block used was about 1.6 litre/min. This optimum gas flow rate is equivalent to a gas flux at the bubble-source diffuser block of 1.9×10^{-4} litre/min/mm². Beyond this gas flux, a significant increase in bubble size was observed.

When comparing the experimental results with the predictions of the math model, it is found that the math model (for $d_B = 0.25$ mm) predicts very similar results for gas flow rates of approx. 1 litre/min and above. Below 1 litre/min the mathematical model predicts much lower removal efficiencies than were measured experimentally. However, this is the expected considering that the math model does not account for particle separation by other mechanisms than bubble attachment, such as simple flotation. As shown in Fig. 15 the baseline case (no bubbling) has a removal efficiency of 45%, whereas the math model predicts 0% separation without bubbling. Consequently at low gas flow rates (i.e. less than 1 litre/min), the math model predicts separation efficiencies that are too low. A promising indication of the utility of the math model is that its prediction of the separation efficiency at the optimum gas flow rate of 1.6 litre/min is in good agreement with the experimental measurement and thus the model may be used to predict optimum gas flow rates.

6.3.2 Influence of Particle Size

In order to determine the influence of tundish bubbling on the separation of different sizes of particles, experiments were conducted with two different particle size distributions; these were 53 to 75 μm (64 μm average) and 75 to 106 μm (90.5 μm average). These size ranges simulate the somewhat smaller size particles that are typically found in liquid steel (see Appendix, Section 9.2). These experiments were performed at a water throughput in the tundish of 27 litre/min. The gas injection rate for gas bubbling was 0.4 litre/min. The results are presented in Fig. 19, where it can be seen that bubbling improved particle separation efficiency significantly as compared to the baseline tundish (no bubbling) for both particle size ranges. Separation efficiencies were 36 and 45% for the baseline tundish and 68 and 85% with bubbling, for the 64 μm and 90.5 μm average particle size ranges respectively. Particle separation efficiency increases with particle size since collision probability increases with particle size (see Fig. 3). Particle separation efficiency is largely a function of collision probability and thus it is expected that separation efficiency should be significantly influenced by particle size.

As shown in Fig. 19, the math model predicts lower separation efficiencies than those measured, particularly for the smaller particles. However as explained previously the mathematical model does not account for separation mechanisms other than particle/bubble attachment such as simple flotation, and as a result at gas flow rates less than the optimum, such as that used for this experiment (0.4 litre/min), the math model is expected to predict lower separation efficiencies than measured.

6.3.3 Influence of Tundish Residence Time

In order to determine the influence of tundish residence time, experiments were performed with water throughputs of 18, 27, and 40.5 litre/min (i.e. simulating 2, 3 and 4.5 ton/min of liquid steel), at a standard gas bubbling rate of 0.4 litre/min using the 90.5 μ m average diameter (75 to 106 μ m range) particles. Increasing the water throughput decreases the mean residence time (τ_T) of the liquid in the tundish. At 18, 27 and 40.5 litre/min, the mean residence time of the water in the tundish is 6.75, 4.5 and 3.0 minutes, respectively. The results of these experiments are presented in Fig. 20.

With bubbling, the experimentally measured separation efficiency, as presented in Fig. 20, varies near linearly over the experimental range of tundish throughput as predicted by the math model. The difference in separation efficiency between the bubbling and non-bubbling experiments is similar at both 27 and 40.5 litre/min. But at the lowest throughput of 18 litre/min, this difference is clearly less as there is a substantial improvement in the flotation efficiency as compared to the higher throughputs without bubbling. The possible reasons for this are three-fold: (1) at the lowest throughput the tundish residence time is sufficient to allow for significantly greater flotation of the larger inclusions in the particle size range, (2) the turbulence created at the inlet is substantially reduced at low throughput and consequently re-entrainment is reduced, and (3) also as a result of reduced turbulence, the flow in the tundish is more plug-like allowing increased particle separation by simple flotation.

As previously discussed in Section 6.3.2, with bubbling gas flow rates less than 1 litre/min the math model predicts lower separation efficiencies than those measured in the water model since the math model ignores simple flotation. As seen in Fig. 20, this effect is again observed in the comparison of the math model predictions to the experimental results regarding the influence of tundish residence time.

6.3.4 Influence of Gas Bubble Size

The math model predicts that the size of the gas bubbles is a very important factor in particle separation. As discussed in Section 3.1 of this thesis, the mathematical model suggests that relatively small bubbles (< 3 mm dia.) would be required in liquid steel to promote high particle separation efficiencies. In order to determine the influence of bubble size, a bubbling block designed to produce relatively large bubbles was fabricated for the water model. The 'large-bubble' bubbling block size was identical to that shown in Fig. 11, but instead of installing a porous ceramic medium into the block, an acrylic plate with an array of 1/16" dia. holes was used. The bubbles produced by this block were found to be ~4mm in diameter.

Flow rates of air below 0.8 litre/min were insufficient to produce an even distribution of bubbles across the bubbling block. Thus experiments were conducted with flow-rates of 0.8, 1.6 and 3 litre/min. The 90.5 μ m average diameter (75 to 106 μ m range) particles

were used for all of the ‘large-bubble’ experiments. The results of these experiments are compared with those previously obtained using the standard bubbling block and no gas bubbling in Fig. 21. At gas flow-rates of 0.8 and 1.6 litre/min, the separation efficiencies are only slightly greater than the no-bubbling baseline, indicating little improvement over no bubbling at all. At the maximum flow-rate of 3 litre/min, the separation efficiency improved to 57%, which is only a marginal improvement when compared to the results of the standard bubble block that provided 97% separation efficiency at the same flow rate. These results confirm the math model prediction that relatively small bubbles are necessary to achieve high particle separation efficiencies in a tundish.

The separation efficiency predicted by the mathematical model for the large bubble size (~4mm) is not shown on Fig. 21, since this model predicts separation efficiencies on the order of only 1%. However as discussed previously, the math model does not account for simple flotation or the increase in the upward velocity of the particles as they pass through the bubble plume. The increase in upward particle velocity induced at the 3 litre/min gas flow rate may be the reason the separation efficiency is higher than that measured at the lower gas flow rates, since this effect not expected to be the result of particle/bubble attachment.

7.0 CONCLUSIONS AND RECOMMENDATIONS

A simple mathematical model of inclusion separation from liquid steel by gas bubbling in a tundish has been developed and compared with the results of physical simulation of tundish bubbling using water and linear low-density polyethylene (LLDPE) particles.

Mathematical modeling predicts that inclusion removal efficiency is maximized as bubble size is minimized. For relatively large bubble sizes (e.g. >3mm) the effect of tundish residence time and the bubbly volume fraction of the tundish can be substantial. Increasing the bubbly volume fraction and longer residence times of the liquid steel in the tundish can increase inclusion separation efficiency, by allowing greater time of contact in the bubbly region and allowing inclusions a longer time to be removed by simple flotation. The model indicates that for high removal efficiencies (>80%) of inclusions less than 60 μm in size bubbles less than 3 mm in diameter should be used. Thus, the development of new technologies for the introduction of tiny gas bubbles into liquid steel is expected to be very helpful to the application of tundish bubbling as a means for inclusion removal enhancement.

The experimental results obtained during physical modeling confirmed that particle separation by gas bubbling in a tundish could be an efficient method for enhancing inclusion separation from the liquid bulk. Particle removal from the liquid by attachment to rising gas bubbles was determined to be far more efficient at separating particles from

the bulk liquid as compared to an impact pad or a floating particle sink. It was also confirmed that relatively small bubbles (< 3 mm in diameter) are required to achieve any reasonable increase in particle separation as compared to that achieved by simple flotation in the absence of gas bubbling. At a bubble size of 0.25mm, an optimum gas flux of 1.9×10^{-4} litre/min/mm² was found to provide excellent particle separation efficiency (95%). A bubble size of 4mm was found to provide only a very minor particle separation improvement as compared to the baseline (no bubbling) case.

The results of this study demonstrate that the use of a gas bubbler in a steel casting tundish, to promote inclusion particle removal and thereby enhance the 'cleanliness' of the steel products, is a promising technology if the small bubble size necessary can be achieved. Thus, the general topic of tundish gas bubbling and the specific topic of new technology for the production (<3mm dia.) gas bubbles in liquid steel should attract further exploration in the future.

8.0 REFERENCES

1. Rogler, J.P, Heaslip, L.J., Xu, D., Mehrvar, M., *AIST Transactions*, 2004, In Press.
2. Rogler, J.P, Heaslip, L.J., Xu, D., Mehrvar, M., *AIST Transactions*, 2004, In Press.
3. Rogler, J.P, Heaslip, L.J., Mehrvar, M., *Canadian Metallurgical Quarterly*, 2004, In Press.
4. Sahai, Y. and Ahuja, R., *Tundish Metallurgy*, Iron and Steel Society, 1990, 89-99.
5. Sinha, A.K. and Sahai, Y., *ISIJ Int.*, 1993, 33, No. 5, 556-566.
6. Brooks, G.A. and Setiadharmaji, W., *Steelmaking Conference Proceedings*, Iron and Steel Society, 1997, 556-662.
7. Yamanaka, H. *Tetsu-to-Hagane* 1983, 69, S213.
8. Zhang, L. and Taniguchi, S., *ISS Transactions*, 2001, 28 (9), 55-79.
9. Nguyen, A.V., Ralston, J., and Schulze, H. J., *Int. J. Min. Process.*, 1998, 53, 225-249.
10. Nguyen, A.V., *Int. J. Min. Process*, 1999, 56, 165-205.
11. Dobby, G. S. and Finch, J.A., *Int. J. Min. Process.*, 1987, 21, 421-260.
12. Nguyen, A.V. and Kmet, S., *Int. J. Min. Process.*, 1994, 40, 155-169.
13. Schulze, H. J., *Mineral Processing and Extractive Metallurgy Review*, 1989, 5, 43-76.
14. Davies, R. M., and Taylor, G.I., *Proc. Royal. Soc.*, 1950, A200, 375.
15. Szekely, J. *Fluid Flow Phenomena in Metals Processing*, Academic Press, 1979, 305-350.
16. Hongbin, Y., Shibata, H., Emi, T., and Suzuki, M., *ISIJ Int.*, 1997, 37, ,10, 936-945.
17. Shibata, H., Yin, H., and Emi, T., *Phil. Trans. R. Soc. Lond.*, 1998. A 356, 957-966.
18. Guthrie, R. I. L. and Irons, G.A., *Metallurgical Transactions*, 1978, 9B, 101-110.

19. Wang, Z., Mukai, K., and Izu, D., *ISIJ Int.*, 1999, 39 (2), 154-163.
20. Okumura, K., Harris, R., Sano, M., *Canadian Metallurgical Quarterly*, 1997, 37 (1), 49-56.
21. Sahai, Y. and Guthrie, R. I. L., *Metallurgical Transactions*, 1982, 13B, 193-201.
22. Fowkes, F.M., McCarthy, D.C., and Mostafa, M.A., *J. Colloid Interface Sci.* 1980, 78, 200-206.
23. Heaslip, L.J., McLean, A., and Sommerville, I.D., *Continuous Casting*, ISS of AIME, 1983, 1, 70-71.

9.0 APPENDIX

9.1 Simulation of Tundish Flow Based on Froude Number Similitude

In order to relate various quantities and measurements in a scaled water model to their associated quantities in the full-scale liquid steel system that is being simulated, dimensionless numbers must be examined in order to determine proper scaling relationships.

In this study, it is desired to simulate buoyant particle separation from liquid steel flowing through a tundish. First, we can consider the modeling of steel flow in a tundish. This flow is driven by gravity force at high Reynolds number. The Reynolds number (N_{Re}) of the flow entering the tundish at a mass flowrate of 3 t/min, through a typical 3” (76mm) diameter shroud can be estimated as follows:

$$Q_L = \frac{3000kg}{min} \cdot \frac{1m^3}{7000kg} \cdot \frac{1min}{60s} = 7.1 \times 10^{-3} m^3 / s \quad (A1)$$

$$u_L = \frac{Q_L}{A_s} = \frac{7.1 \times 10^{-3}}{\left(\frac{\pi}{4} \cdot 0.076^2\right)} = 1.57 m / s \quad (A2)$$

$$N_{Re} = \frac{u_L \cdot \rho_L \cdot L_c}{\mu_L} = \frac{1.57 \cdot 7000 \cdot 0.076}{0.007} = 1.2 \times 10^5 \quad (A3)$$

The Reynolds number is a measure of the ratio of inertial forces to viscous forces in the flow and thus $N_{Re} > 10^5$ indicates that the flow in a tundish is dominated by inertial effects. Thus in a steel casting tundish, the flow is gravity driven and inertially dominated. The Froude number gives a ratio of the inertial force to the gravitational

force. In accordance with the derivation of relations of similitude presented by Heaslip et al. [23], for Froude similarity between the model and the prototype, the Froude number in each system must be equivalent;

$$N_{Fr} = \frac{U^2}{gL} \quad \text{and thus} \quad N_{Fr_m} = N_{Fr_p} = \frac{U_m^2}{L_m} = \frac{U_p^2}{L_p} \quad (A4)$$

Where the subscript m denotes the model and p denotes the prototype.

Rearranging Equation (A4):

$$\frac{L_m}{L_p} = \frac{U_m^2}{U_p^2} \quad \text{or} \quad L_f = U_f^2 \quad (A5)$$

Where equation (A5) considers $L_f = L_m/L_p$ as the length scale ratio and $U_f = U_m/U_p$ as the velocity scale ratio. Thus, equation (A5) defines the relationship between the velocity scale and the length scale in accordance with Froude number similitude. The time scale can be defined with the aid of the following equation:

$$t_f = \frac{L_f}{U_f} \quad (A6)$$

Substituting equation (A5) into equation (A6) provides us with a relationship between the time scale and length scale as follows:

$$t_f = \sqrt{L_f} \quad (A7)$$

Similarly, a flow-rate scale can be derived from the length scale and time scale as:

$$Q_f = \frac{L_f^3}{t_f} \quad (A8)$$

Substituting equation (A7) into (A8) yields the following relation between the flow-rate scale and the length scale:

$$Q_f = L_f^{5/2} \quad (A9)$$

Thus, to simulate a mass flow-rate of 3 ton/min of liquid steel in a water model of 1/3rd scale, with similarity based upon Froude number equivalence, equation (A9) can be used to determine the scaled flow in the model as follows:

$$Q_f = (1/3)^{5/2} = 0.064 \quad (A10)$$

$$Q_m = 0.064 \cdot Q_p = 0.064 \cdot (7.1 \times 10^{-3}) = 4.54 \times 10^{-4} \text{ m}^3 / \text{s} = 27 \text{ litres} / \text{min} \quad (A11)$$

9.2 Simulation of Particle Rise Velocity Based on Stoke's Law

Also important to this study is the rise velocity of the particles, which may be predicted by Stoke's Law. For a 1/3rd scale model with Froude number similitude (as discussed in Appendix 9.1), the particle rise velocity in the prototype and the model are related by the following equation:

$$U_F = \frac{U_{R-P}}{U_{R-M}} = \sqrt{3} \quad (A12)$$

The rise velocity of a particle in liquid is calculated with Stoke's Law:

$$U_R = \frac{d_p^2}{18\mu} g(\rho_L - \rho_G) \quad (A13)$$

In the full scale Steel/Alumina system the equation is as follows:

$$U_{R-P} = \frac{d_{P-S}^2}{18\mu_s} g(\rho_S - \rho_{AL}) \quad (A14)$$

In the 1/3rd scale model water/LLDPE system, the equation is as follows:

$$U_{R-M} = \frac{d_{P-W}^2}{18\mu_W} g(\rho_W - \rho_{PE}) \quad (A15)$$

Now combining equations (A12), (A14) and (A15):

$$U_F = \frac{d_{P-S}^2 \cdot (\rho_S - \rho_{AL})\mu_W}{d_{P-M}^2 \cdot (\rho_W - \rho_{PE})\mu_S} = \sqrt{3} \quad (A16)$$

The density values and viscosity values are entered below:

$$\frac{d_{P-S}^2 \cdot (7.05 - 2.80)0.001}{d_{P-M}^2 \cdot (1.00 - 0.92)0.007} = \sqrt{3} \quad (A17)$$

Thus the particle sizes in the full-scale liquid steel/alumina system and the water/LLDPE system are related by the following equation:

$$\therefore d_{P-S} = 0.478 \cdot d_{P-M} \quad (A18)$$

Thus, the full-scale particle size distributions modeled are 25 to 36 μ m (53 to 75 μ m in the model) and 36 to 51 μ m (75 to 106 μ m in the model).

9.3 Simulation of Oxide Inclusion Concentration in Liquid Steel

The oxide inclusion concentration in liquid steel can be estimated using the total oxygen concentration of the melt. The total oxygen concentration is the sum of the dissolved oxygen (oxygen atoms in the liquid metal) and the oxygen in non-metallic inclusion particles suspended in the liquid steel. As liquid steel cools and solidifies, oxygen solubility is reduced to near zero and thus the total oxygen content finally reports as non-metallic oxides. For a steel to be termed ‘clean’, the total oxygen concentration

should be less than 30 to 50ppm. Assuming these oxides are alumina (Al_2O_3), the mass fraction of oxygen is approximately 50%. Thus, the concentration of alumina in liquid steel with a total oxygen concentration of 40ppm will be 80ppm. It is desired to use a similar concentration of LLDPE particles in the water model. The liquid volume in the water model tundish at the operating level of 330mm is 123 litres (0.123 m^3). Thus 6g of particles in this volume would represent a concentration of:

$$\frac{6 \text{ g particles}}{0.123 \text{ m}^3 \text{ water}} \times \frac{1 \text{ m}^3 \text{ water}}{1000000 \text{ g water}} = 4.88 \times 10^{-5} \text{ g particles / g water} \cong 49 \text{ ppm}$$

Such a concentration of inclusions (49ppm) falls into the category of ‘clean’ steel. Thus using this concentration in the model allows us to see if the cleanest of steels could be cleaned further.

9.4 Dimensionless Parameters

The following equations are used in calculation of the dimensionless parameters referenced in Section 2 of this thesis.

$$A = \frac{u_p}{u_B} + \frac{d_p}{d_b} X + \left(\frac{d_p}{d_b} \right)^2 M \qquad B = \frac{d_p}{d_b} \frac{Y}{A} + \left(\frac{d_p}{d_b} \right)^2 \frac{N}{A}$$

$$C = \frac{u_p}{u_B} \left(\frac{d_b}{d_p} \right)^2 \qquad D = \frac{\sqrt{(X+C)^2 + 3Y^2} - (X+C)}{3Y}$$

$$M = -\frac{9}{4} - \frac{27 \text{ Re}}{64} + 0.2266 \text{ Re}^{1.1274} \qquad N = -0.437 \text{ Re}^{1.0562}$$

$$X = \frac{3}{2} + \frac{9 \text{ Re}}{32 + 9.888 \text{ Re}^{0.694}} \qquad Y = \frac{3 \text{ Re}}{8 + 1.736 \text{ Re}^{0.694}}$$

9.5 Analysis of Polyethylene Particles

To investigate properties of the polyethylene (PE) sample a number of tests were conducted. These tests include, high-temperature GPC (gel permeation chromatography), DSC (differential scanning calorimetry), and CRYSTAF (crystallization analysis fractionation). The results of these tests are presented below.

High-temperature GPC:

Average molecular weight results for the sample tested are summarized in Table A1. All values are within expected range. The sample is fairly narrow. Its PDI (polydispersity index) is around 3.5. PDI is the ratio of M_w over M_n , it is a measure of how broad the molecular weight distribution of the sample is.

Table A1: Average molecular weights of LLDPE sample

	Conventional (GPC) calibration	Universal (GPCV) calibration
M_n (kg/mol)	15.1	16.71
M_w (kg/mol)	54.4	59.07
M_z (kg/mol)	142.4	162.26
PDI	3.6	3.54

Based on GPC results, it seems that the PE sample is likely linear. From Figure A1, the observed and fitted intrinsic viscosity curves coincide with each other. The fitted curve is based on viscosity of linear chains. If there is significant amount of branching in the sample, the observed viscosity curve is expected to deviate from the fitted one, since branched chains have lower elution volume and lower viscosity.

DSC:

The percent crystallinity of the sample was determined using DSC (differential scanning calorimetry). The heat of crystallization of the sample was obtained. By comparing sample results to heat of crystallization of a theoretically 100% crystalline polyethylene, the sample's percent crystallinity was determined to be about 38.46%. The onset of the melting of the sample started at 53.47°C. T_m (melting temperature) for this sample was 122.24°C.

CRYSTAF:

Base on the CRYSTAF results in Figure A2, the sample displayed a profile that is typical for Ziegler-Natta catalyzed polyethylene. The first peak to the right (narrow peak) is for linear chains, whereas the second represents chains that contain co-monomer. The exact nature of co-monomer cannot be known unless other tests are conducted (e.g. NMR). The peak crystallization temperature for chains containing co-monomers is about 62°C. Crystallization temperature for linear chains peaked around 80°C. These linear chains contribute most to the overall crystallinity of the sample.

Concluding remarks:

This sample seems to be a linear polyethylene with narrow molecular weight distribution. Since this sample is linear, its percent crystallinity is expected to be higher than 38%. But that was not the case. This is most likely due to the existence of co-monomer. Copolymers lead to short chain branches that interfere with formation of crystal lamella. The exact type of co-monomer used requires further investigation.

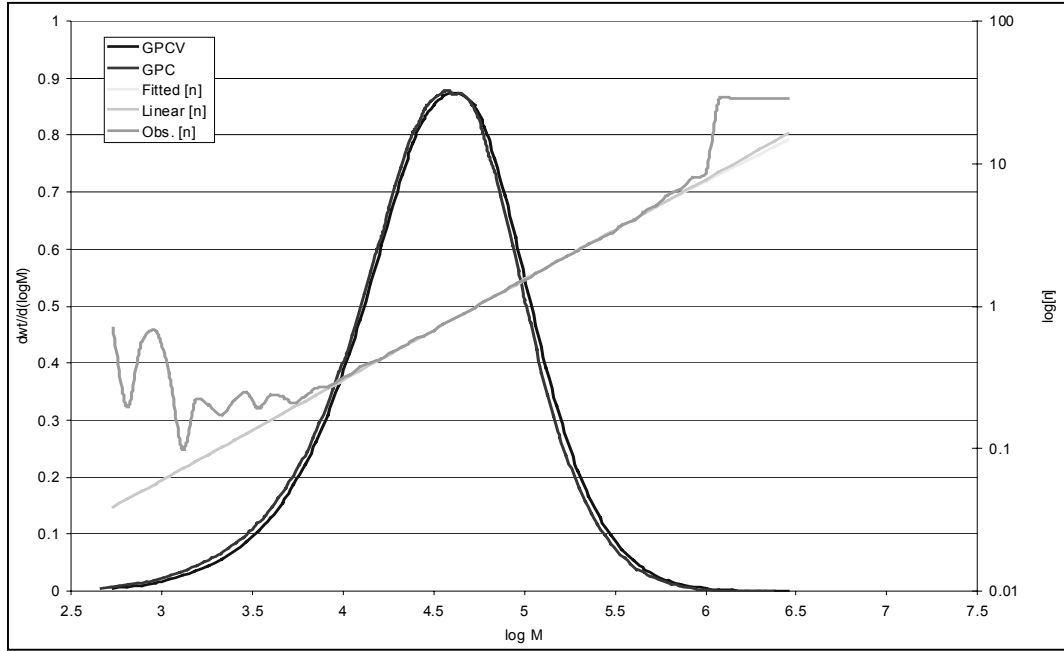


Figure A1: Comparison of GPC Results

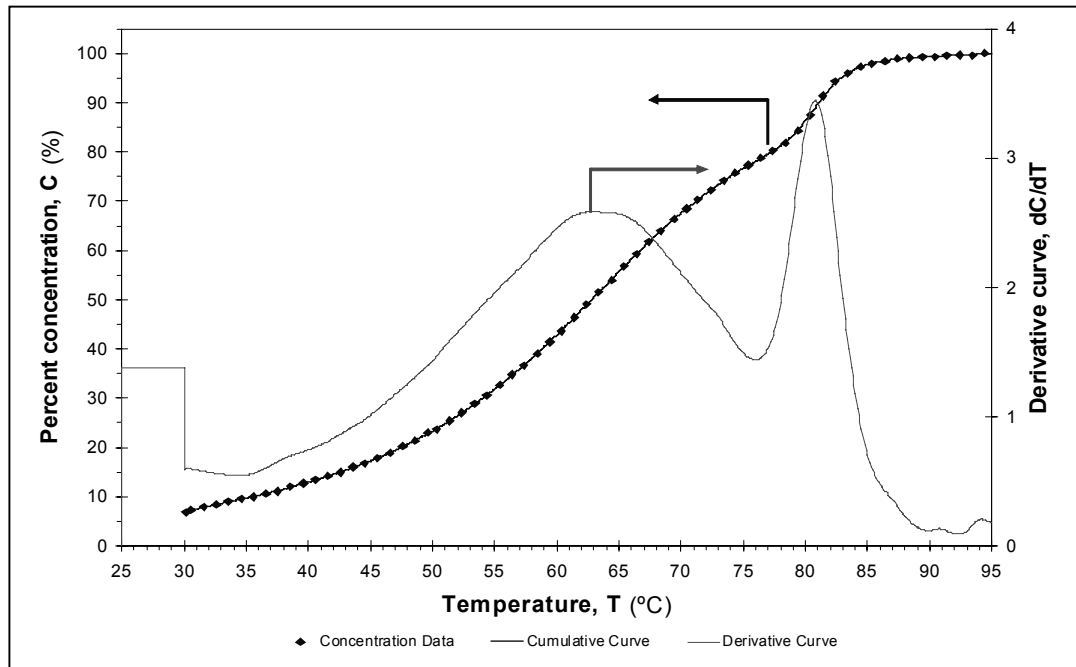
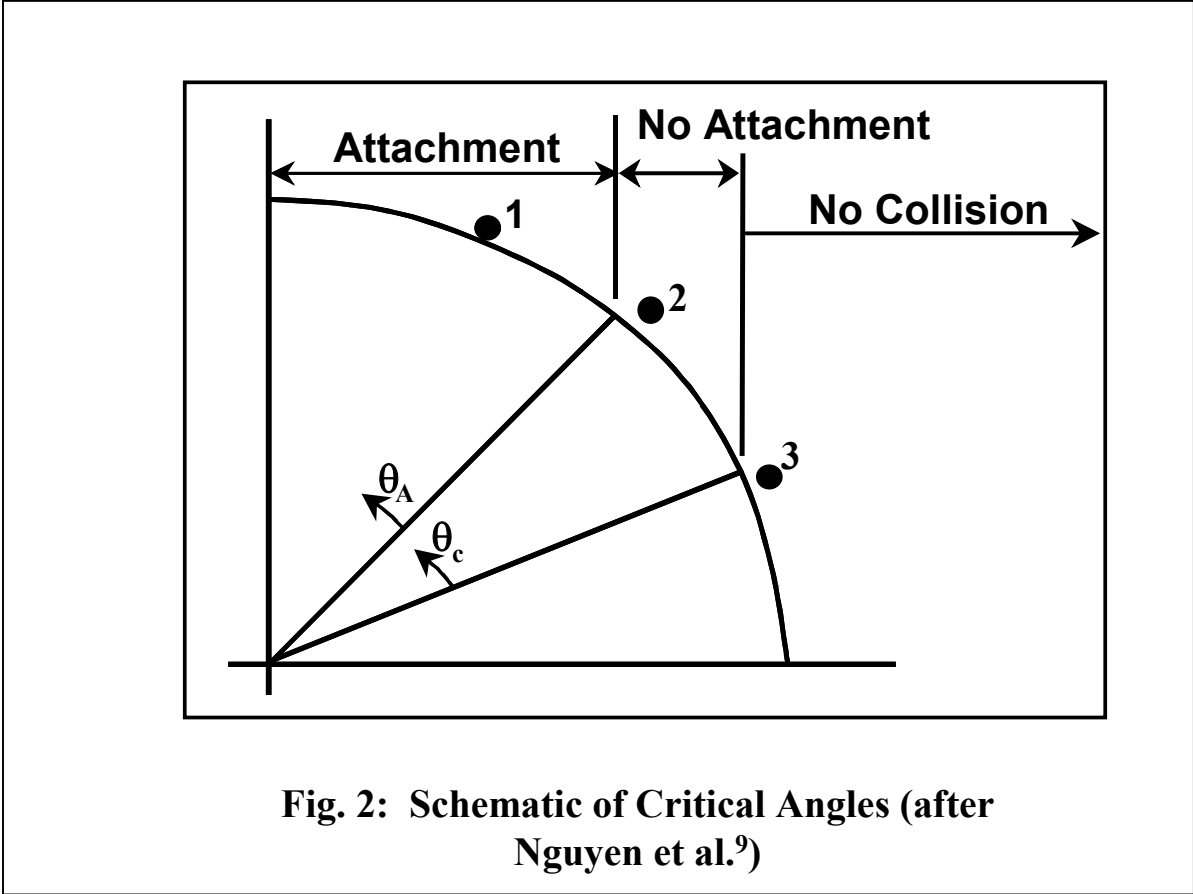
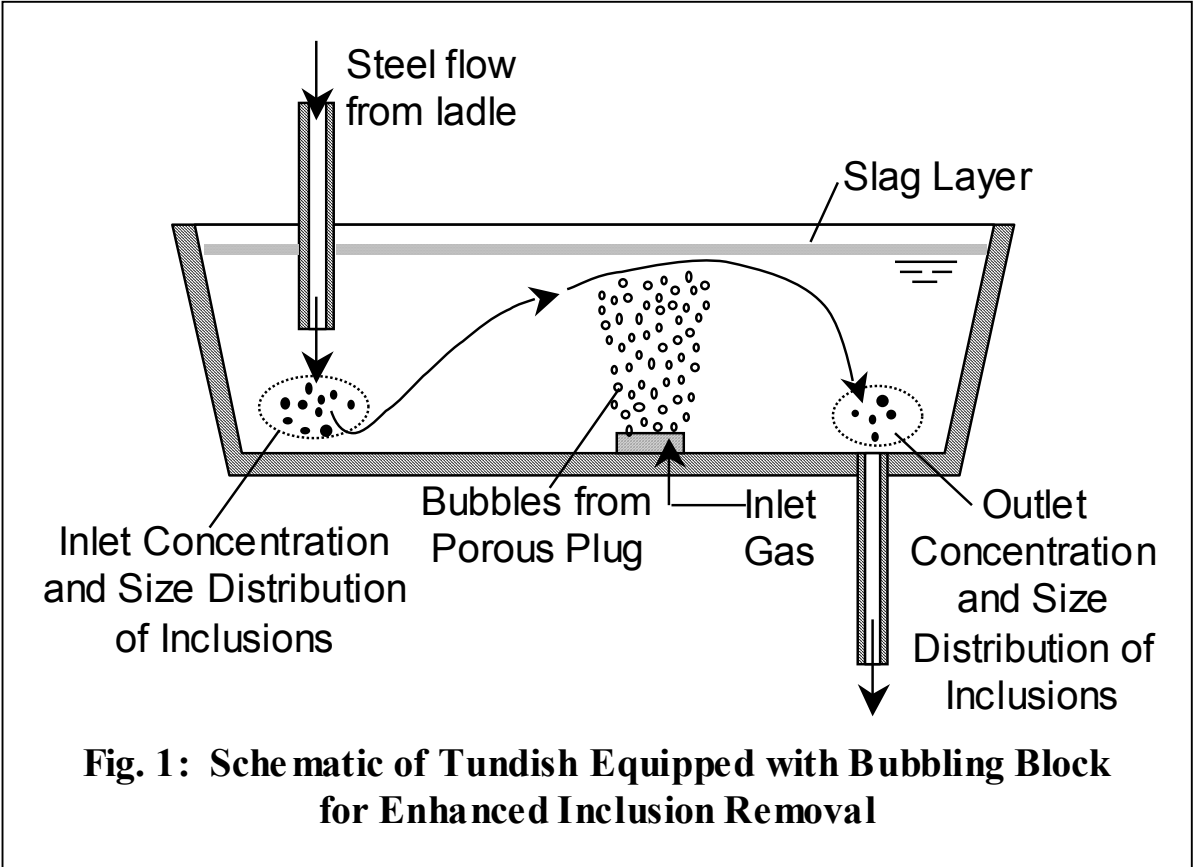
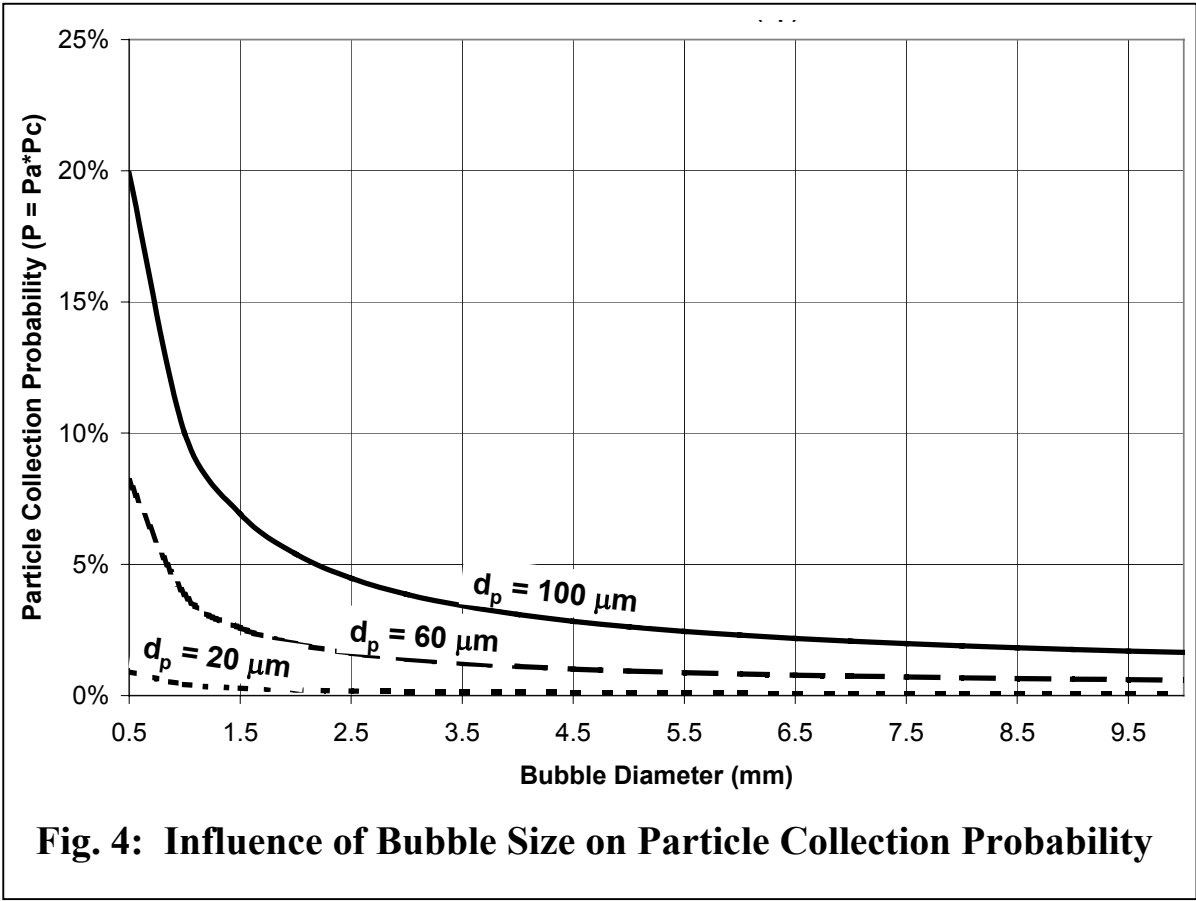
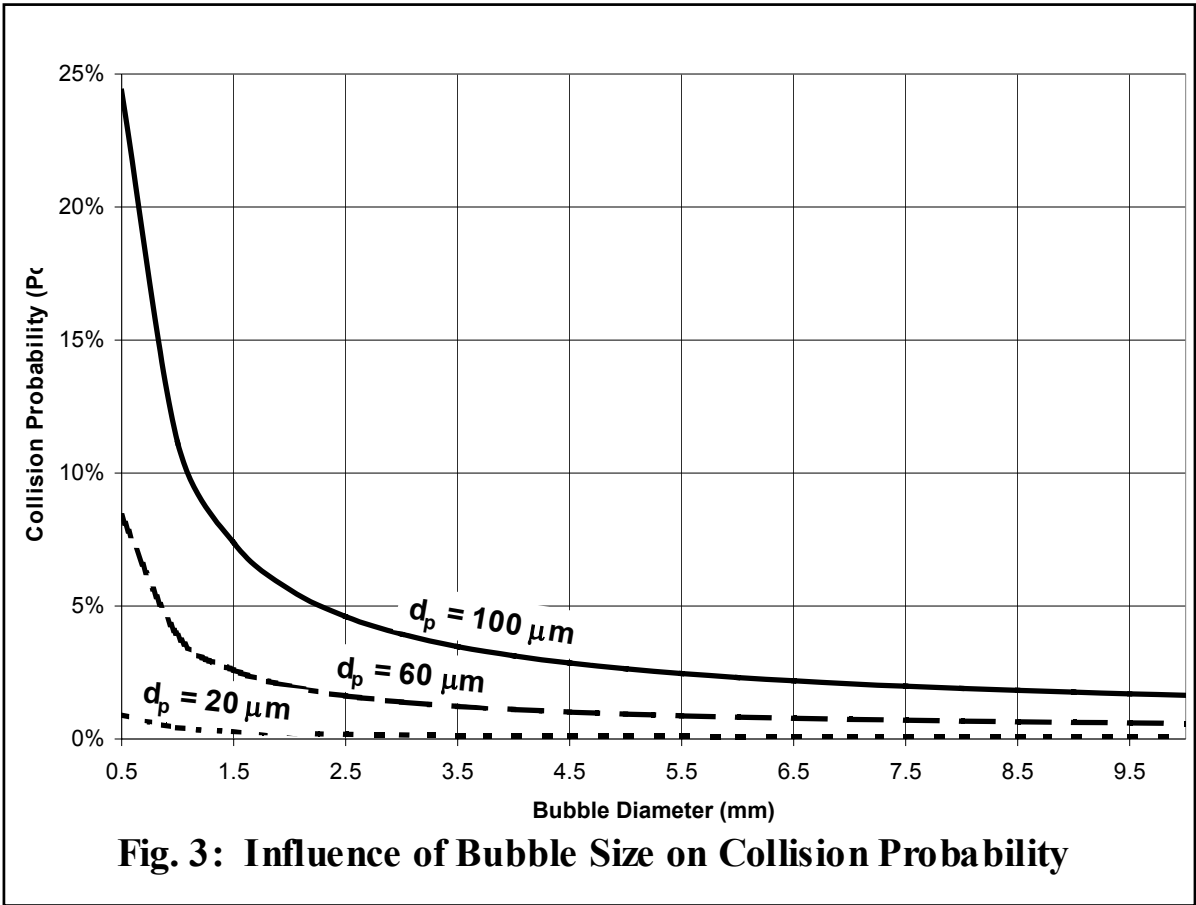
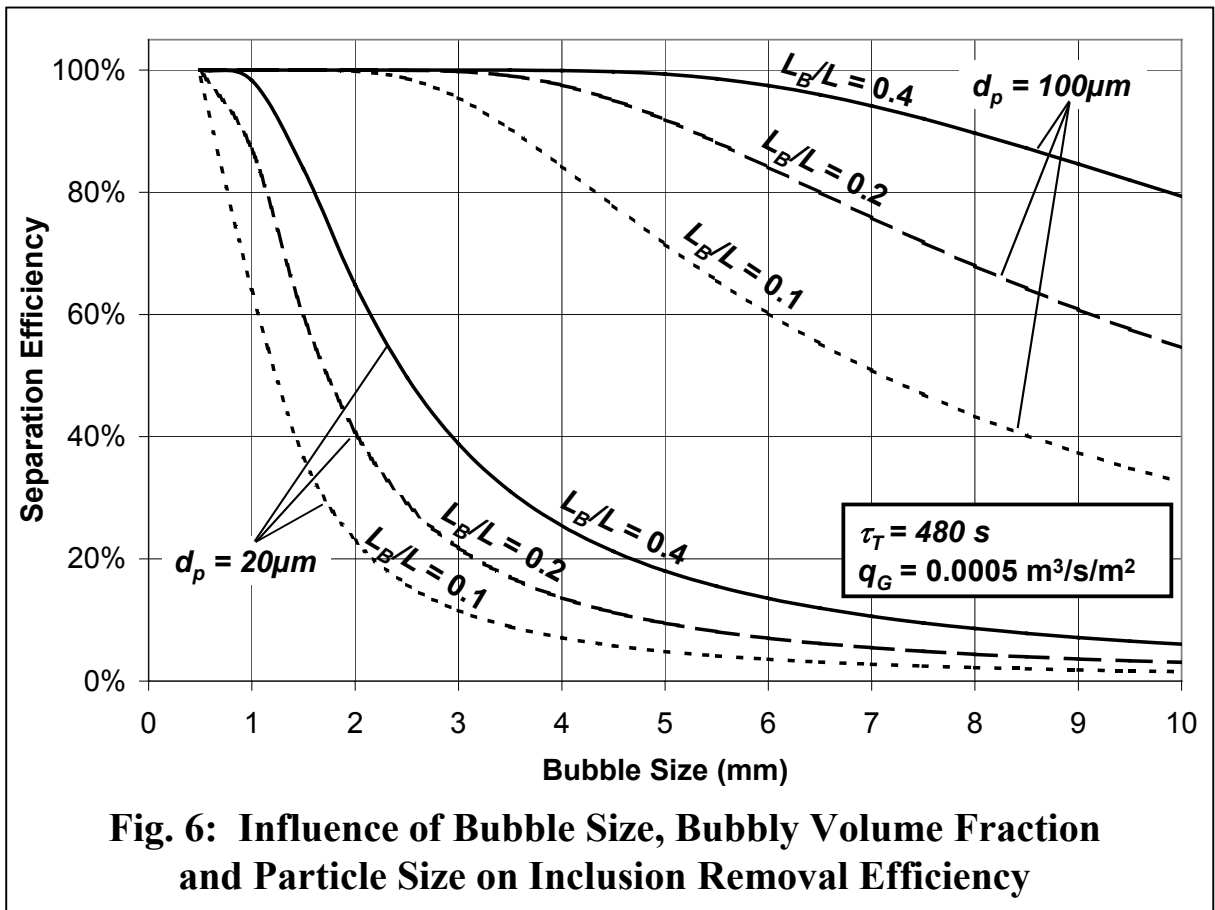
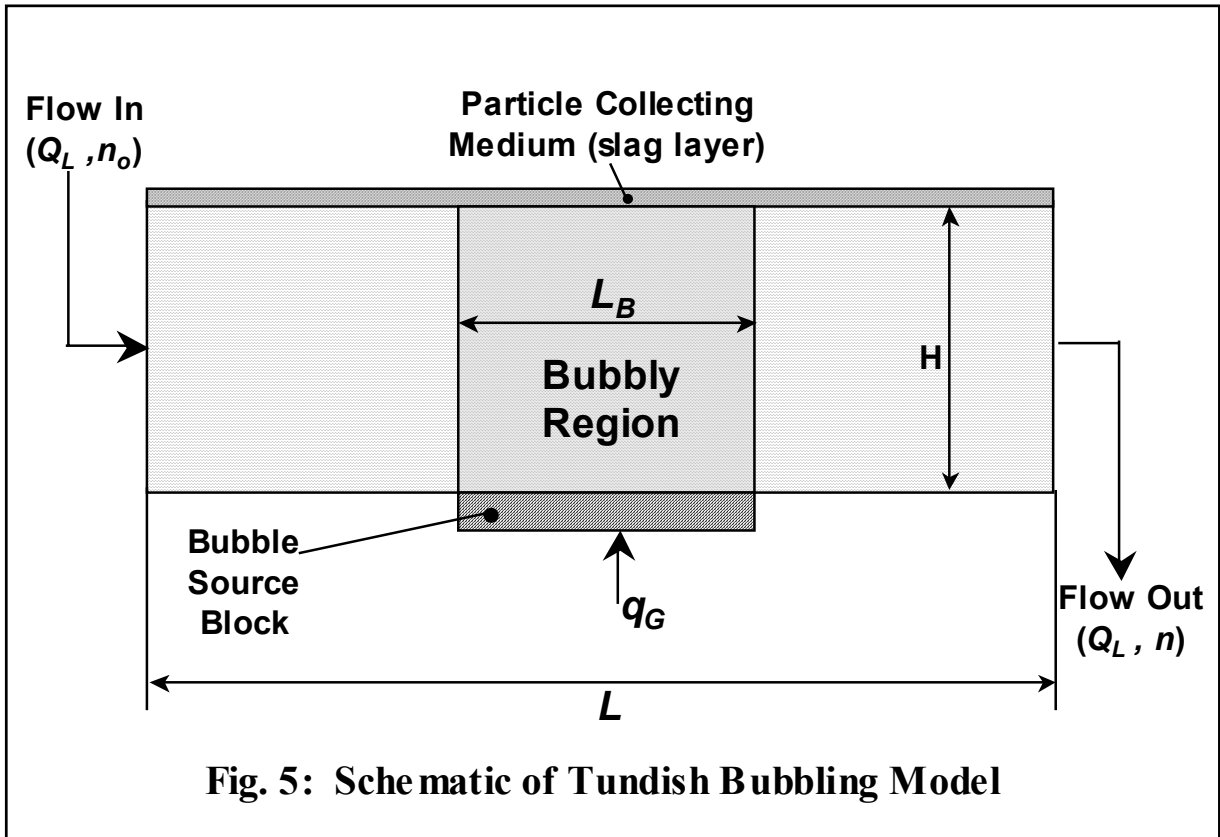


Figure A2: CRYSTAF Results







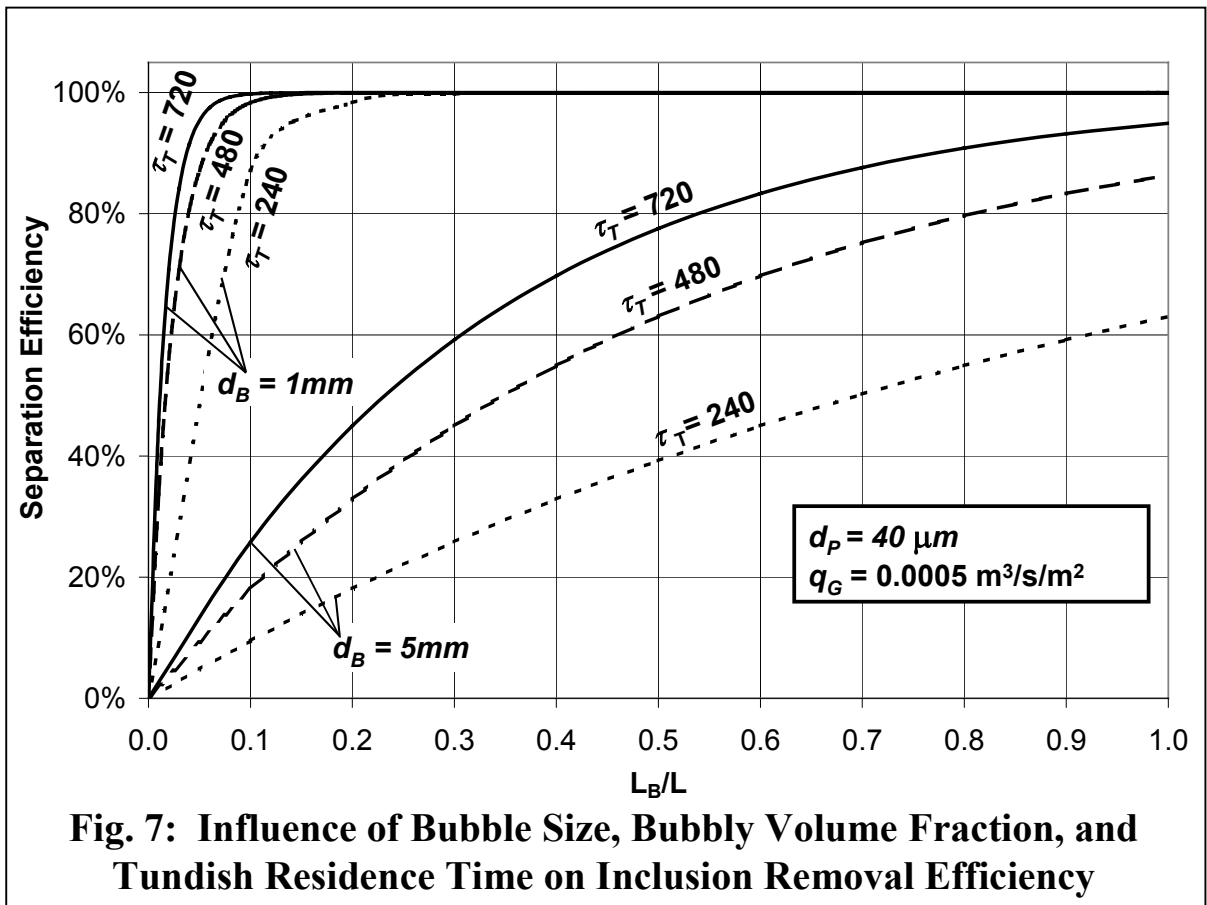


Fig. 7: Influence of Bubble Size, Bubbly Volume Fraction, and Tundish Residence Time on Inclusion Removal Efficiency

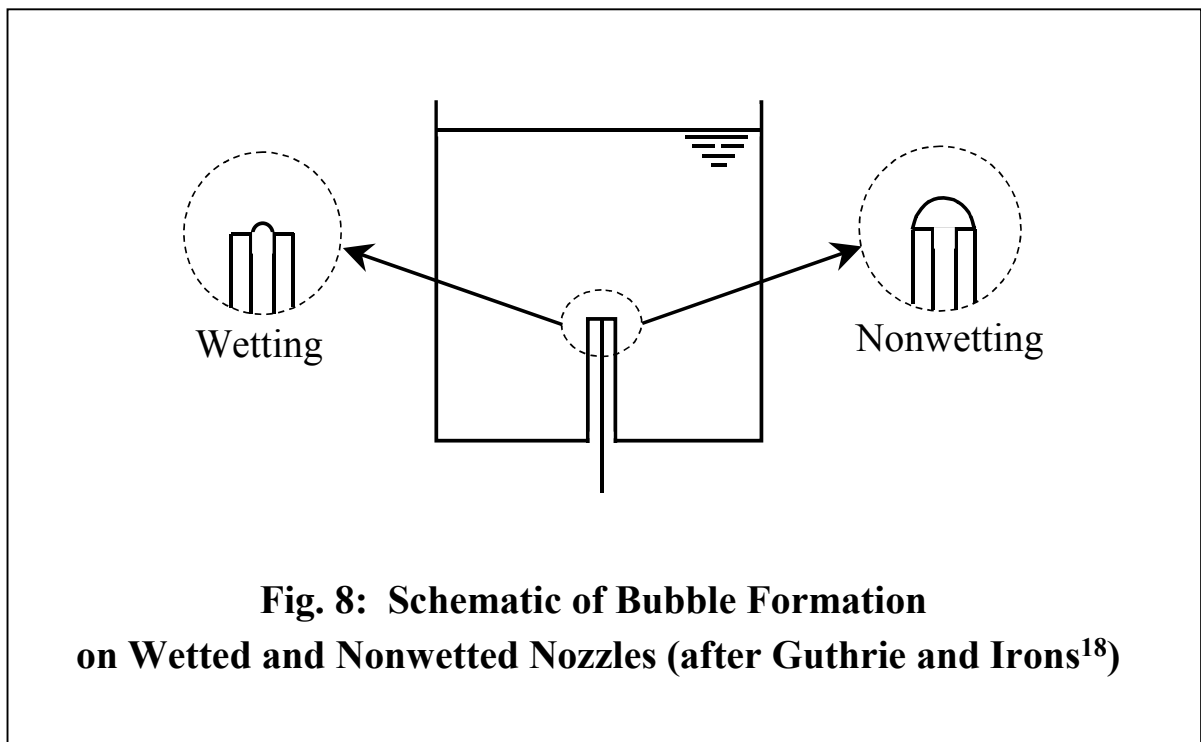
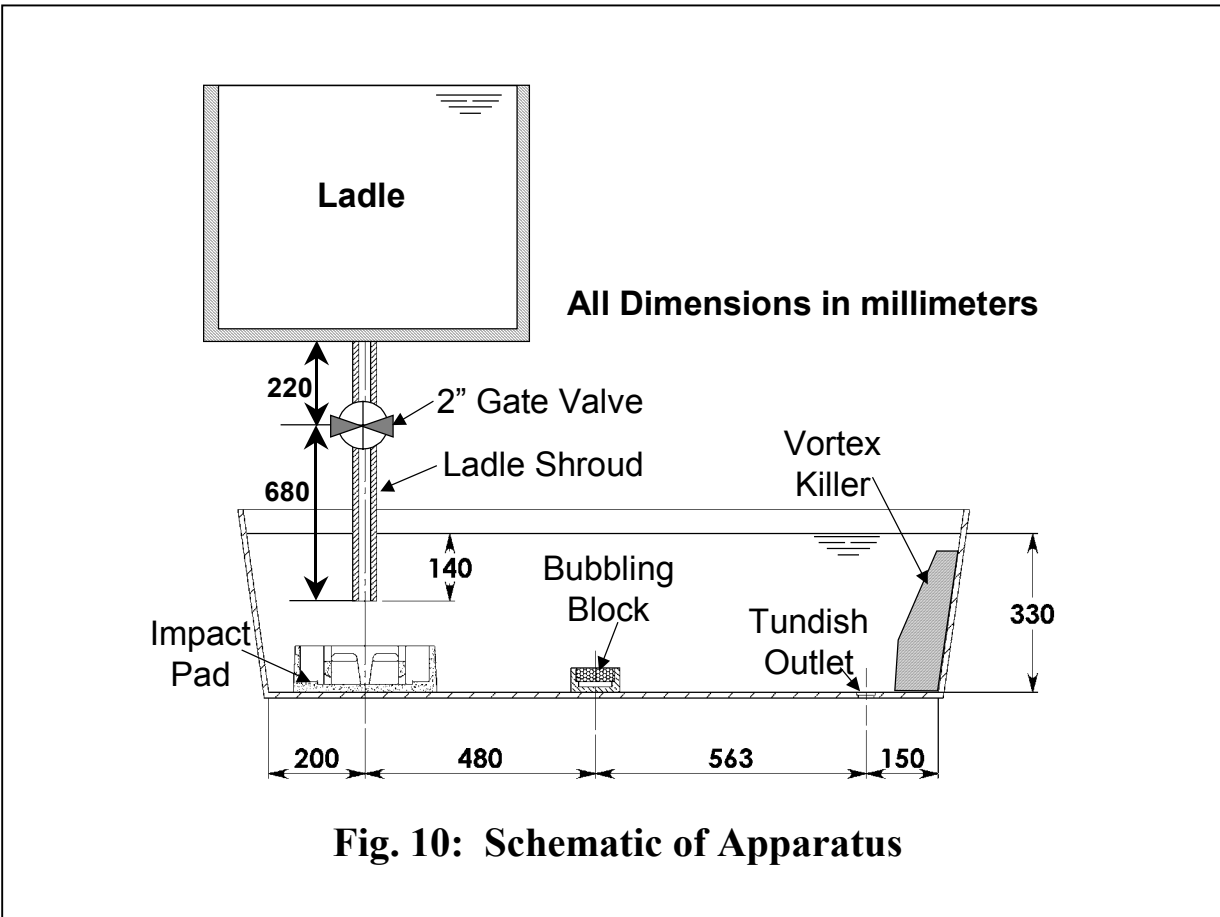
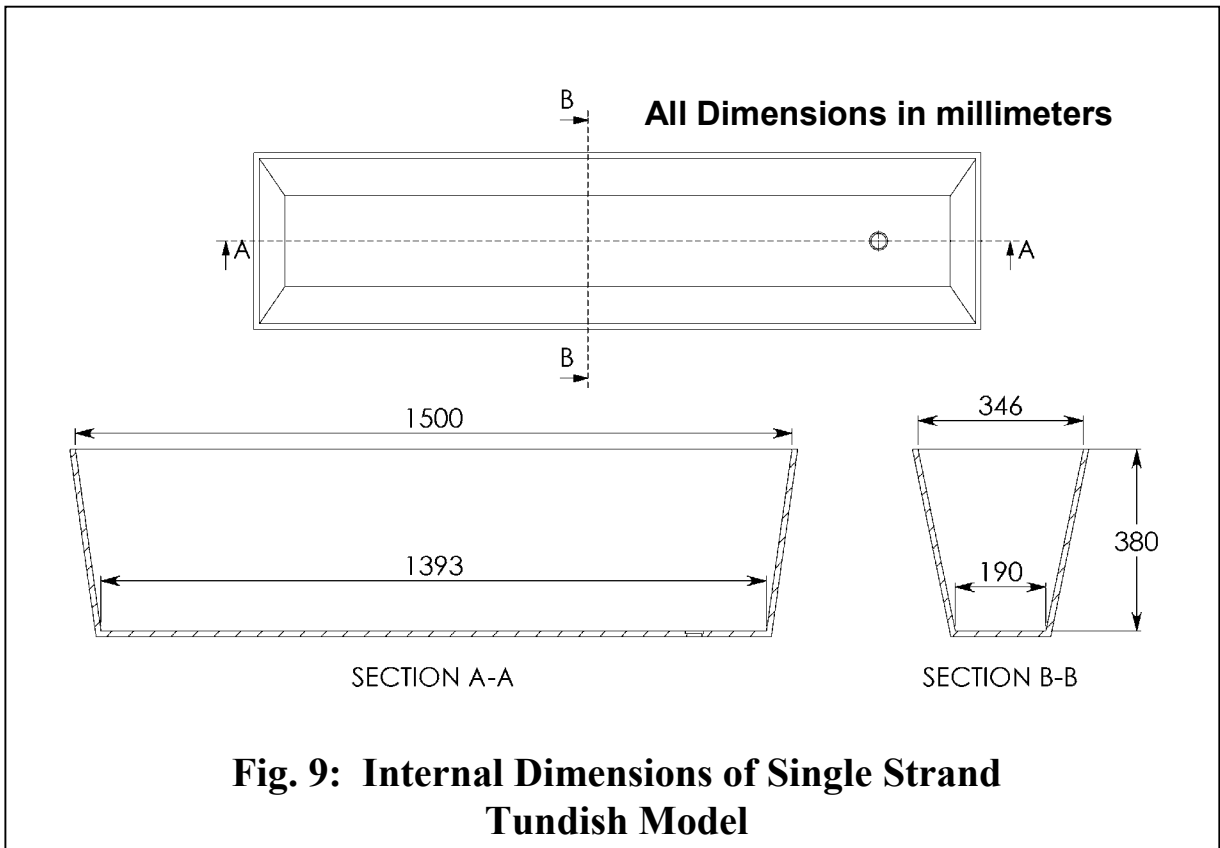
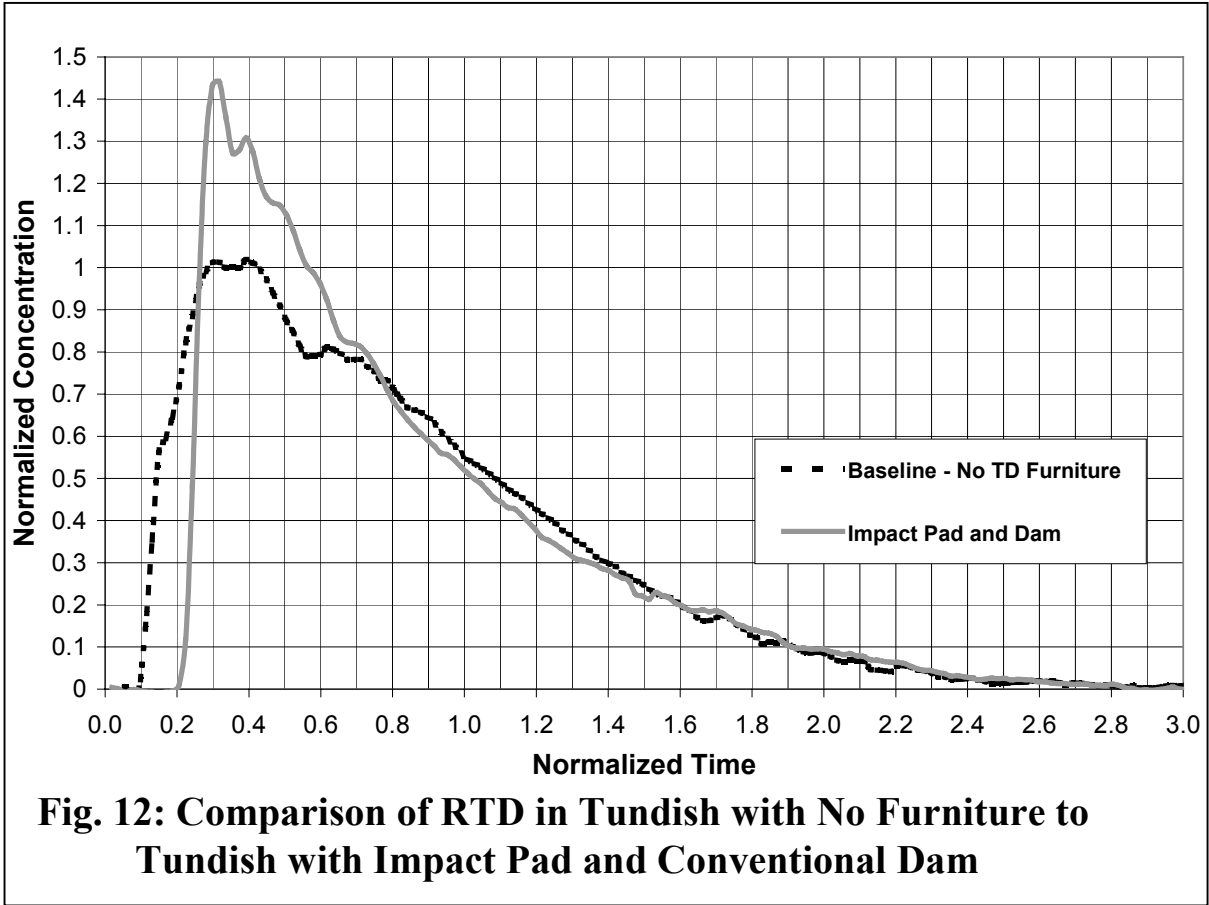
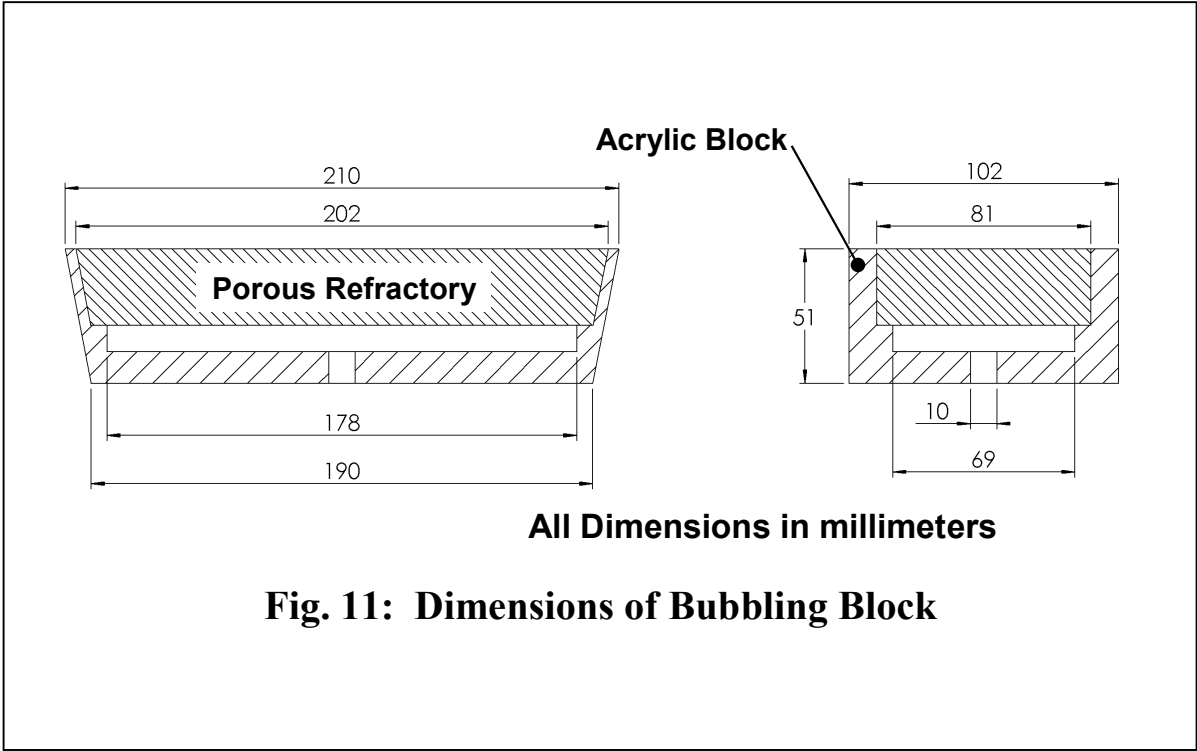
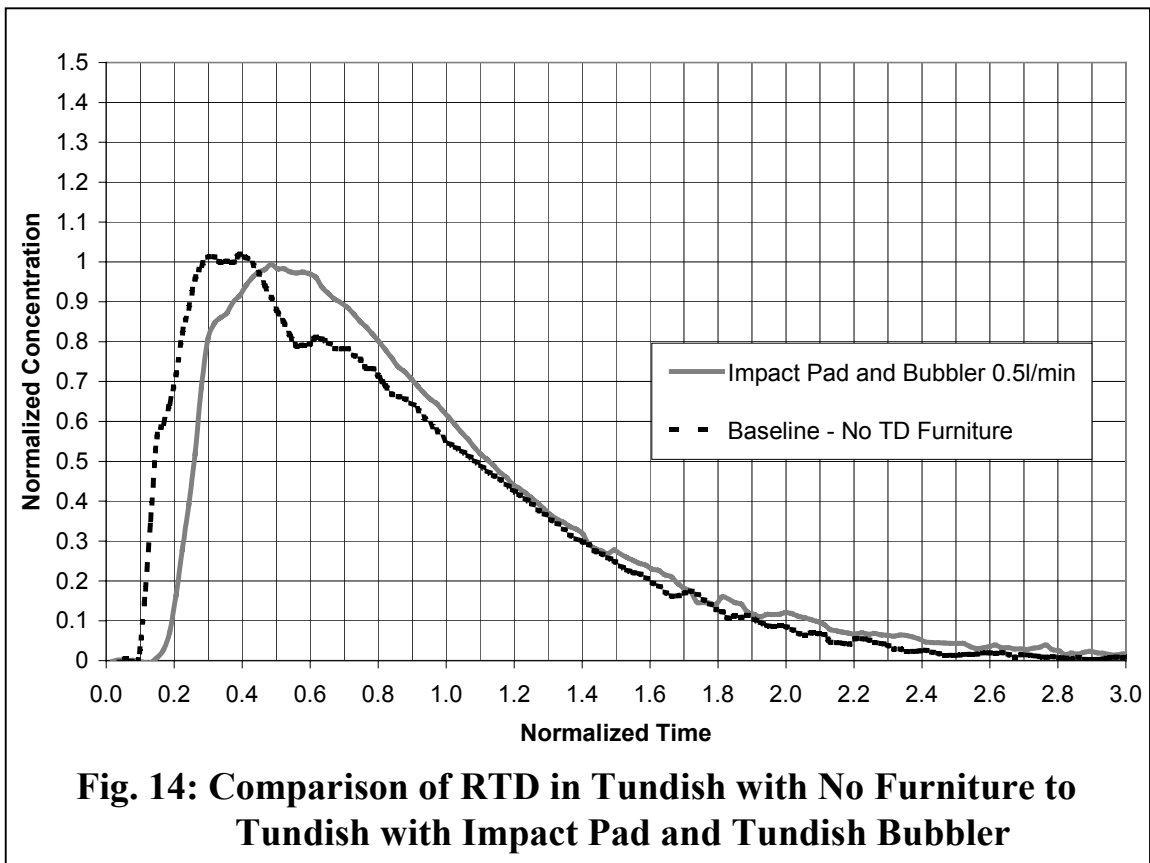
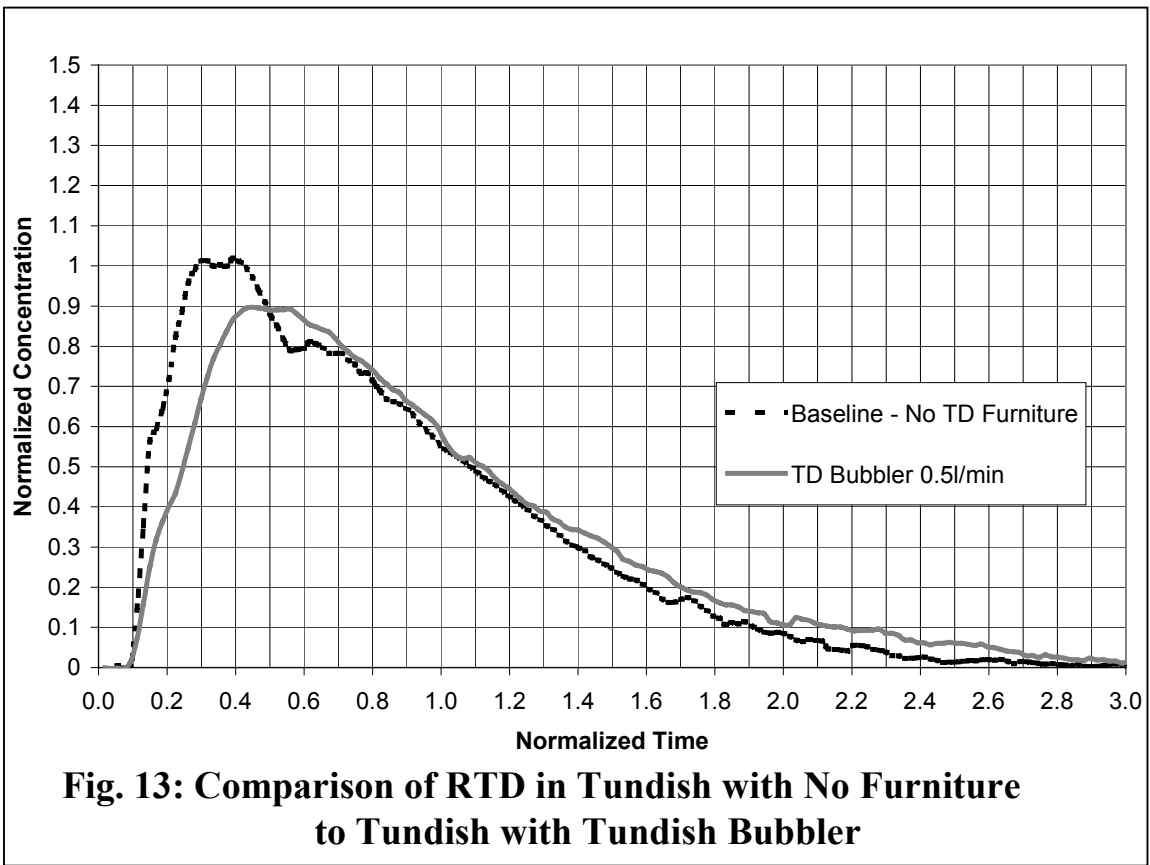
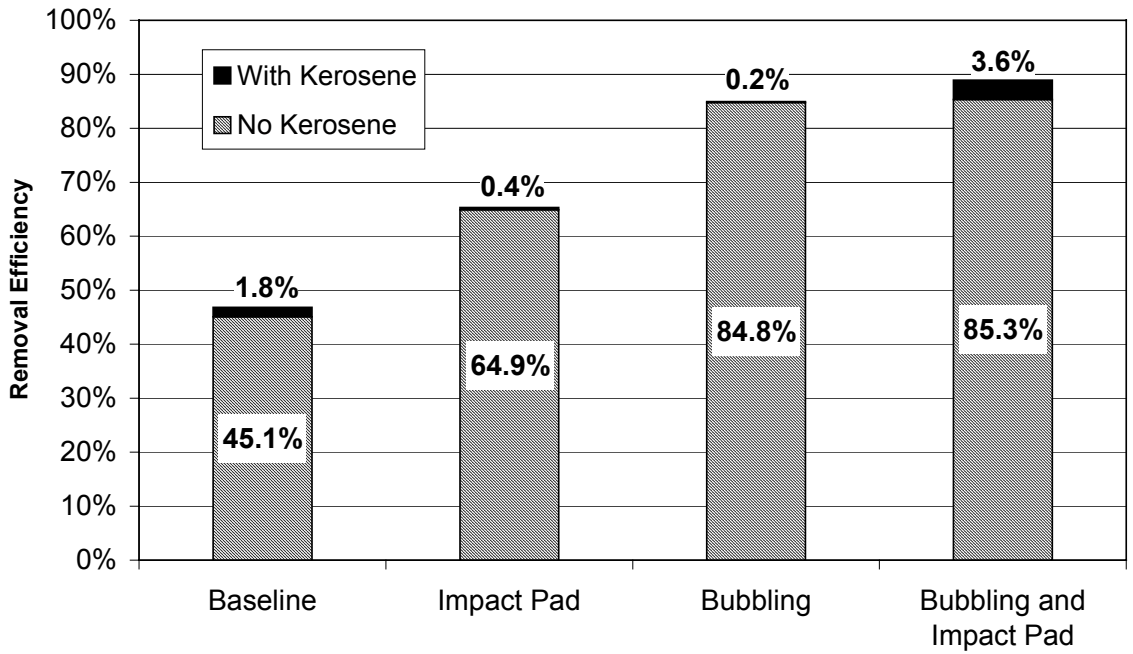


Fig. 8: Schematic of Bubble Formation on Wetted and Nonwetted Nozzles (after Guthrie and Irons¹⁸)



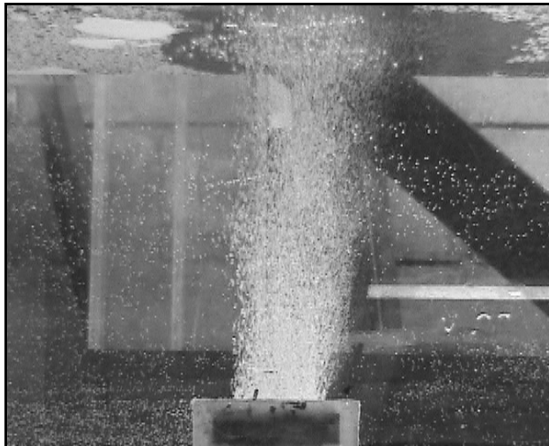




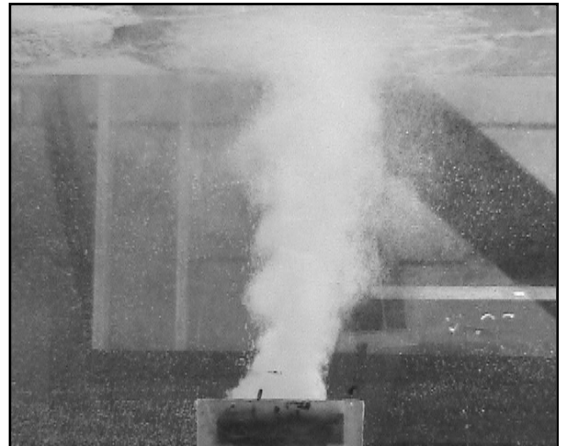


Average Particle Size = 90.5 μ m, $L_B/L = 0.036$, Bubble Size = 0.25mm, Gas Injection Rate = 0.4l/min, Simulated Throughput = 3t/min

Fig. 15: Results of Primary Experimental Matrix



Bubbles Before Interaction with Particles



Bubbles During Interaction with Particles

Fig. 16: Comparison of Bubbles Before and During Interaction with Particles

